UNIVERSITY OF CALIFORNIA, IRVINE

Flexible and Stretchable Wearable Sensors for Human Motion and Physiological Monitoring

DISSERTATION

submitted for the degree of

DOCTOR OF PHILOSPHY

in Chemical Engineering

by

Sun Jun Park

Dissertation Committee :

Professor Michelle Khine, Chair

Professor James Earthman

Professor William Tang

2017

DEDICATION

To

My parents Sang Eon Park and Myoung Ok Lee

My Sibling Sunju Park and her family Dong Hyun Baek and Jiwon Baek

&

My family Sumi Lee and Jayden Siyul Park

TABLE OF CONTENTS

LIST OF FIGURES

ACKNOWLEDGEMENTS

I would like to express my deepest gratitude to

My family for providing love and support,

My friends for providing perspective

My colleagues for providing ideas and inspiration

My Mentor, Professor Michelle Khine for guiding and challenging me.

CURRICULUM VITAE

Sun Jun Park

EDUCATION

2017 Ph.D, University of California, Irvine
Chemical Engineering
Thesis :
2009 MS, Hanyang University, South Korea
Chemical Engineering
2007 BS, Hanyang University, South Korea
Chemical Engineering

PUBLICATIONS

• Sun-Jun Park, Joshua Kim, Xiaoran Li, Jamie Le, and Michelle Khine
Flexible Capacitance Pressure Sensor for Continuous Blood Flow Monitoring *(In Preparation)*

• Lancy Lin, Michael Chu, Sun-Jun Park, Jasmine Zhang, Alexa Nazarian and Michelle Khine
Highly Wrinkled Metal Thin Films for Wearable Health Monitoring *(In Preparation)*

• Sun-Jun Park, Joshua Kim, Michael Chu and Michelle Khine.
Flexible Piezoresistive Pressure Sensor using Wrinkled Carbon Nanotube Thin Films for Human Physiological Signals. *Advanced Materials Technologies (2017)*

• Sun-Jun Park , Joshua Kim, Michael Chu and Michelle Khine
Highly Flexible Wrinkled Carbon Nanotube Thin Film Strain Sensor for Detecting Human Movement. *Advanced Materials Technologies (2016)*, 10.1002/admt.201600053

• Jonathan D. Pegan, Jasmine Zhang, Michael Chu, Thao Nguyen, Sun-Jun Park, Akshay Paul, Joshua Kim, and Michelle Khine
Skin-Mountable Stretch Sensor for Wearable Health Monitoring, *Nanoscale (2016)*, 26, 11, 1678

• Joshua Kim, Sun-Jun Park, Thao Nguyen, Michael Chu, Jonathan D. Pegan, and Michelle Khine
Highly Stretchable Wrinkled Gold Thin Film Wires, *Applied Physics Letters (2016)*, 108, 061901

INTELETUAL PROPERTY

- U.S Provisional Application Serical No : PCT/US2015/031442, "Fetal Health Monitor"
- U.S Provisional Application Serical No : 62/316,375, "Vital Signs Monitor"
- U.S Provisional Application Serical No : 62/296,361, "Highly Wrinkled Metal Thin Films Using Lift-Off Layers"
- U.S Provisional Application Serical No : 62/147,979 (PCT/US2015/031438), "Densification of One Dimension Nanostructures Via Uniaxial or Multiaxial Shrinkage"

PRESENTATIONS

The Wearable Biomedical Systems and Sensors, *WEAR Conference 2017*, San Francisco, California. June 12-14, 2017

Flexible Wrinkled CNT Pressure Sensor for Detecting Human Motion & Physiological Signals, *2017 UCI-UCLA Student Research Workshop & Symposium sponsored by Broadcom Foundation*, Irvine, California, May 10-11, 2017

Highly Stretchable, Skin-Like, Sensors and Electronic Components, *Center for Advanced Design and Manufacturing of Integrated Microfluidics (CADMIM)*, Mar.1-2, 2017

Flexible Wrinkled CNT Pressure Sensor for Detecting Human Physiological Signals, *EMBS Micro and Nanotechnology in Medicine Conference*, Waikoloa, Hawaii, Dec. 12-16, 2016

Super Flexible and Stretchable Wrinkled Carbon Nanotube Thin-Film Strain and Pressure Sensor to Monitor Human Movement and Physiological Signals, *MRS Fall 2016*, Boston, Massachusetts, Nov. 27-Dec. 2, 2016

Wrinkled Metal Thin Film Sensors for Wearable Health Monitoring, *SoCal Micro and Nanofluidics Symposium*, Irvine, California, Sep.1-2, 2016

AWARDS & HONORS

- 2017 UCI-UCLA Student Research Workshop & Symposium sponsored by Broadcom Foundation(2017)
- 1st Place Award, Most Innovative Research Presentation and Best Poster Presentation. (3 Awards)
- Calit2 at UCI Engineering Graduate Fellowship Program sponsored by Broadcom Foundation (2016-2017) Ability to conduct research devices for Internet of Things (IoT) and smart devices.
- 1st Place on Oral Presentation (KSEA-SWRC 2016)
- 2nd Place on ChEMS prospective student visitation day poster session (2014)
- Best Teaching Assistant Award (Fall quarter 2013)

ABSTRACT OF THE DISSERTATION

Flexible and Stretchable Wearable Sensor for Human Motion and Physiological Monitoring

by

Sun Jun Park

Doctor of Phiolosophy in Chemical Engineering

University of California, Irvine, 2017

Professor Michelle Khine, Chair

With the growing prominence of wearable electronic technology, there is a need to improve the mechanical reliability of electronics for more demanding applications. However, currently available devices have limits on stretchability, flexibility, portability and high cost because of their functional materials. Therefore, there is a critical need to develop conductive materials that can withstand repeated large strain, pressure and can be manufactured into discreet, low cost, and dense arrays with high stretchability, flexibility, and sensitivity.

This research presents a shape memory polymer embedded highly flexible and stretchable wrinkled carbon nanotube thin film wire. We preassemble CNTs on a shape memory polymer substrate with wrinkles, to demonstrate significant densification, improvement of stretchability and high electrical performance followed by the shrinking of the substrate. And we transferred to Ecoflex or PDMS thin films which utilized as wearable and skin-mountable strain sensor and pressure sensor for human motion and physiological signals detection. Unlike pre-existing sensors, these wrinkled CNT strain and pressure sensors can be worn conformal to

human skin and are capable to endure higher strains and pressure. The piezoresistive response of shrink induced wrinkled CNT thin films demonstrated conductive performance in excess of high strain and pressure. Also the wrinkled CNT wires exhibited consistent performance after repetitive stimulus. Importantly, these wrinkled thin films are inexpensive to fabricate and are compatible to conventional manufacturing processes. In this proposal, we focus on this wrinkled CNT concept toward practical applications in flexible and highly sensitive sensor for monitoring human physiological signals as wearable sensors which relates to the health of individuals.

CHAPTER 1: Introduction

1.1 Current State of the art of wearable sensors

There is a growing need to improve the mechanical reliability of flexible electronics as the demand for 'wearable' applications in health and medical monitoring increases. These new wearable electrical components must conform to soft curvilinear surfaces, stretch and flex with the body's motion, and be lightweight and unobtrusive. It is critical to overcome rigid, brittle, and largely planar electronics and sensors to develop more insightful investigation for human body monitoring.[1,2] Flexible electronics will fulfill the growing interest in long term monitoring systems for personalized fitness, physical rehabilitation, finger sensing micro switches, entertainment devices, and continuous health monitoring for various parameters such as blood pressure, breathing and body temperature.[3–9]

Wearable strain sensor devices are designed to be mounted on the human skin to measure the strain induced by muscle movements. Many sensors transduce the mechanical deformation to a resistance change upon stretching and releasing. This phenomenon is known as the piezoresistive effect. The relative change in resistance, $\Delta R/R_0$, is related to the mechanical strain ε by the gauge factor (GF) according to Equation 1.[1]

$$GF = \frac{\Delta R / R_0}{\varepsilon} \tag{1.1}$$

In order to be an effective strain sensor for monitoring human motion, the sensors must have high flexibility and stretchability, while maintaining high sensitivity, or high GF values,

across a large dynamic range. For example, high gauge strain sensors are able to measure both the small and large angle deformations inherent to human joint motion. Thus, there has been a large amount of research in developing highly stretchable and sensitive wearable strain sensors by using micro/nanostructured thin films, functional materials, and elastomeric substrates.

Micro and nanostructures have also been implemented to improve the elasticity of brittle materials.[10–12] These micro/nanostructures are typically generated via buckling from compressive substrates. For example, researchers have deposited brittle materials onto pre-strained silicon rubbers and released the strain to create wavy buckled structures. These wavy buckled structures provided strain relief for brittle materials rendering them stretchable.[13,14]

Typical wearable strain sensors consist of patterned metallic thin films on flexible elastomeric substrates. Recent developments in creating highly stretchable wearable strain sensors used nanoscale metal thin films,[15] nanoparticles,[16] nanowires (NWs),[17–19] nanotubes,[20–26] and graphene.[27–31] For example, Kang et al. utilized brittle platinum thin films to achieve high sensitivity (GF>2000), but the strain sensor was only able to withstand strains of up to 2%.[32] Li et al. investigated graphene woven fabric for strain sensing (GF ~1000), but was still limited to a maximum strain of 6%.[33] Conversely, Yan et al. reported highly stretchable graphene-nanocellulose nanopaper that can stretch out to 100% strain, but the strain sensor only had a GF of 7.1.[34]

Another popular functional material that is used for strain sensing is carbon nanotubes (CNTs). Percolating networks of CNTs on flexible elastomeric substrates have been reported to have electromechanical stability under high strain due to the robust contact between individual CNTs.[35] CNT thin films have also shown the ability to bend repeatedly without fracturing.[36–40] Therefore, percolating networks of CNTs have the potential to be used as highly stretchable

strain sensing devices. For instance, Yamada et al. made aligned CNT thin film on PDMS and showed 280% strain but low sensitivity (GF<0.82)[25] and Lipomi et al. investigated spring like structures in the nanotube that reach 150% strain with good conductivity.[22] Ryu et al. showed that aligned CNT fibers grown on flexible substrates were able to stretch out to 900% having GF of up to 47.[41] However, this process required highly ordered alignment of CNT fibers using intricate dry spinning methods.

Furthermore, human motion sensor should have the ability of measuring the spatial distribution of the stress induced by multiple mechanical stimuli such as normal pressure, lateral strain, as it allows object manipulation, grasp control, and recording of body movement such as heart beating, blood pressure.[42,43] Pressure sensors are attractive candidates for promoting the advancement of science and technology in modern society. Flexible pressure sensors based on resistance change, which combine unique advantages of flexibility, have emerged as a highly active field due to their promising applications in artificial intelligence systems and wearable health care devices.

Piezoresistive pressure sensors operate by decreasing the electrical resistance between two electrodes by increasing the number of contact points. The pressure sensitivity of a device is characterized with the following equation:

$$S = \frac{\Delta R / R_0}{\Delta P} \tag{1.2}$$

where R is the resistance, Ro is the initial resistance, and P is pressure

In the past decade, the development of artificial skin based on pressure sensors arrays on flexible substrate has achieved great progresses, reporting increasing sensitivity, response speed, and resolution of tactile mapping.[44,45] But unlike human skin, these pressure sensor arrays lacked stretchability and were limited to the function of providing information of spatial pressure distribution. To solve these problems, the developing of intrinsically stretchable materials and new architecture design of functional materials on sensors are effective strategies to fabricate stretchable pressure sensors.[34] For example, Suh et al developed a skin-attachable pressure sensor based on nanoscale mechanical interlocking between metal-coated nanofibers, the reversible interlocking of these conductive nanofibers enable the detection of pressure, shear, and torsion.[46] Bao and co-workers provided a stretchable mechanical sensor capable of sensing pressure by sandwiching a porous rubber layer and air gap between two stretchable carbon nanotube film electrodes.[47]

Recently, based on the geometric structuring strategy, a stretchable pressure sensor has been reported by Kim et al, in which various sensing elements were integrated on a stretchable serpentine silicon nanoribbon networks. [43] Despite the high performance obtained, the large area fabrication of this highly integrated pressure sensor based on silicon nanoribbon is complicated and expensive, which would hinder its practical and wide application.

1.2 Overview of the dissertation

The dissertation is structured as follows. In chapter 2, fabrication method of self-similar hierarchal wrinkled structures in metal thin films which are created via heat induced biaxial shrinking on shape memory polymers (SMP), such as polystyrene(PS) is demonstrated.[48] The

wrinkles occur due to the mismatches in stiffness between the SMP and the deposited material during the shrinking process.[49] In chapter 3, carbon nanotube (CNT) as a functional material for strain and pressure sensor is introduced. Deposition methods of functional material such as CNT and Au metal are discussed. In Chapter 4 flexible and stretchable silicone based elastic polymer such as Ecoflex and polydimethlysiloxane (PDMS) is introduced for improving wearable strain and pressure sensor. Chapter 5 demonstrated that mats of deposited CNTs on the SMP also result in densified, self-similar nano to microfeatured wrinkles upon shrinkage and showed that these wrinkled CNT thin films can be transferred from the rigid SMP carrier film into Ecoflex 0030. (Smooth-On, PA). The tight entangled CNTs introduce strong van der Waals forces between CNTs to enhance stretchability. Finally we demonstrate highly stretchable strain sensors to detect human motion. In Chapter 6. using the same shrinking fabrication process, highly structured and elastic carbon nanotube thin films as rough conductive electrodes for piezoresistive pressure sensor is developed. Highly wrinkled carbon nanotube thin film electrodes were coupled face-to-face to produce piezoresistive pressure sensors. By incorporating highly wrinkled structures into CNT thin films, pressure sensitivities were improved 12800 fold. We conclude with a discussion of future direction of capacitance based flexible pressure sensor work to enable more successful translation of wearable pressure sensor for human physiological signals in Chapter 7.

To our knowledge, this is the first demonstration of wrinkled CNT thin films by shape memory polymers (SMP), which were integrated in a stretchable human motion and physiological sensor.

CHAPTER 2: Wrinkled Structures by Shape Memory Polymer

2.1 Wrinkled Structure

Wrinkles are observed in everyday life from micro to macro scale such as human skin, nature (mountain ridge). A lot of researcher have been fascinated with wrinkles as a pervasive natural phenomenon.[50,51] When a stiff thin film which is supported by a compliant thick substrate is compressed to a critical in-plane strain, the flat surface loses their stability and forms out of plane deformation such as wrinkles.[52] These wrinkle structures have been studied extensively both theoretically[53,54] and experimentally.[55,56] In early years, theses wrinkles were considered as a failure on fabrications, so most of the studies have focused on how to avoid the wrinkles on the structures. [57]

In recent years there has been a growing interest in intentionally forming these wrinkle structures and leveraging them for creative uses. For example, interest in polymeric wrinkles are increasing as complex quasiperiodic structures are becoming important in cell studies applications.[58] Flexible integrated circuits have taken advantages of the wrinkled structures to fabricate flexible microelectronics as wearable system and using thin wrinkled films of single crystalline silicon based on elastomer substrates,[59,60] Wrinkle are used as a template to direct the assembly of particles[61] or assist in the ordering of liquid crystals.[62] By controlling the formation of the wrinkled structures on a surface, it can change the optical,[63] adhesive properties.[64] These can be applied in molecular detection, filters/sorter, high surface area conductor and actuator even metrology.[65,66] Also in microfluidics, it can be used as a means to open and close channels for fluid flow by tuning surface adhesion and wettability.[59]

2.2 Wrinkling using polymer

Lots of researcher have been developed the ways to form wrinkles on their functional materials. Bowden et al. deposited metal onto a thermally expanded polydimethylsiloxane (PDMS) polymer by cooling the PDMS which causes a compressive stress and from wrinkles about 30mm length on the deposited metal film.[52] Watanabe et al have developed simply pre-stretching the PDMS sheet to and deposit thin film on top and release the PDMS sheet to form 6–20mm striped patterns.[67] Lacour et al. used same method to create stretchable gold electro conductors.[15] Also, Yoo et al. formed polystyrene buckling of by applying a physical mold during the buckling process which have achieve high resolution(<2 mm periodicity) buckles than previously reported.[68] But the process requires complicated microfabrication molding process and takes several hours to form the wrinkles.

2.3 Shape Memory Polymer

Shape-memory polymers are a rising area of active polymers that have dual-shape capability. They can change their shape from A to shape B while shape B is given by the initial processing step and shape A is called programming which is determined by applying a process. This shape-memory effect is not an intrinsic property, that means polymers need external stimuli. Shape memory results from a combination of polymer morphology and specific processing and can be explained as a polymer functionalization. For example, extruding or injection molding, the polymer is in its initial, permanent shape B. Afterwards, in a process called programming, the polymer sample is deformed and fixed into the temporary shape A. Upon application of an external stimulus, the polymer recovers its initial permanent shape B. Shape memory

polymers(SMPs) undergo and return from a significant macroscopic deformation state to their original shape induced by appropriate external stimuli such as heat(temperature change), light, electricity, magnetism, and moisture. This recovery and programming cycle can be repeated several times, with different temporary shapes in continuous cycles. Comparing with metallic alloy shape-memory, this cycle of programming and recovery can take place in a much shorter interval time and polymers allow a much higher deformation rate between shapes A and B.[69]

2.4 Nano/micro wrinkles using Shape Memory Polymer

Here, we have developed a rapid and unique fabrication method to create metal thin film into nanowrinkles of tunable amplitude and wavelength and demonstrable utility on a shape memory polymer,[70] pre-stressed polystyrene (PS) sheets commercially available as the children's toy Shrinky-Dinks. Our approach only needed just leveraging the stiffness mismatch of materials. Our method has ability to rapidly form various regularly-spaced patterns on a large surface, without the use of expensive machineries or complicated lithography processes. We developed a simple and ultra-rapid two-step (metal deposition and subsequent heating) method to controllably create nanometer-scale metal wrinkles. Wrinkles arise from competition between the elastic bending energy of a stiff functional material which is deposit on top of the SMPs and the elastic energy of deformation of the soft substrate on which it is SMPs in this case.

Deposition of CNT and metals onto polymers should consider temperature constraints and the growth dynamics of the metal film. Especially with polystyrene SMPs, the processing temperature threshold is 100^{o}C which is the glass transition temperature of the polmer. Spray

coating of CNT and low temperature physical vapor deposition methods such as sputter deposition and ebeam evaporation for metal can produce high quality metal thin films on SMPs.

Initially, CNT (or metal) was deposited on pre-stressed polystyrene (PS) (KFS50-C, Grafix Arts) sheets. The CNT (or metal) /PS sheet was placed into a convection oven for heat approximately to 150^{o}C to induce biaxial shrinking and form wrinkling into the CNT thin film. The initial PS sheet was shrunk to 33% of initial size and forms CNT (or metal) wrinkles.

CHAPTER 3 : Carbon Nanotube as a Wearable Sensor Material

3.1 Carbon nanotube

The state-of-the-art research in the nanotube forms of materials is huge interest in their synthesis methods, properties study and attempts to the real product industrial applications. Nanomaterials are defined by its materials the sizes o in the 1–100 nm range.[71] They can divided by their shapes into zero-dimensional (0D) and one-dimensional (1D) nanostructures. 0D nanostructures are, for example, quantum dots.[71] Quantum dots were used as a structural material for multiple applications including memory system, quantum lasers and optical sensing materials. However, many of nanotube properties are drastically different from the carbon itself. Therefore nanotube/nanostructures should be considered as a new material with unique physical and chemical properties showing good promising application for a wide range.

Carbon nanotubes (CNT) have a great number of application fields such as composite polymers, catalysts, display, gas sensor, energy conversion, lithium battery conversion, energy storage, sensors etc..[72–74]The great variety of the good mechanical, electrical and magnetic properties of nanotubes can become the starting point for the future nano-electric materials. The use of CNT in sensor devices is one of their most promising applications in electronics. These sensors should have high sensitivity and selectivity, as well as fast response and recovery.

Carbon nanotube is a tubular form of carbon with diameter as small as 1nm and few nanometer to micrometer length. CNT is configurationally equivalent to a two dimensional graphene sheet rolled into a tube. The properties of CNT depend only on tube diameter and chiral angle. For a random chirality distribution, 1/3 of the nanotubes are metallic. What is novel

about CNT is due to the different electrical and thermal conductivities they shows when their hexagonal structures are oriented differently. For example, armchair, chiral and zig-zag structure allow the CNT to acting like metal, semiconductor and insulator, respectively. Carbon nanotube has sp^2 bonds which are stronger than the sp^3 bonds, provide unique strength with honeycomb lattice structure, and 1-D cylindrical structure that allows outstanding mechanical, electrical, and thermal properties.[35–38]

3.2 CNT as a sensor material

As a nanotube is a surface structure, its whole weight is concentrated in its surface layers. This feature is the origin of the uniquely large unit surface of tubulenes which in turn predetermines their electrochemical and adsorption properties.[72] The high sensitivity of the electronic properties of nanotubes to molecules adsorbed on their surface and the unparalleled unit surface providing for this high sensitivity make CNT a promising starting material for the development of super miniaturized chemical and biological sensors.[73,74] The operation principle of these sensors is based on changes in the V–I curves of nanotubes as a result of adsorption of specific molecules on their surface. The use of CNT in sensor devices is one of their most promising applications in electronics. These sensors should have high sensitivity and selectivity, as well as fast response and recovery.

3.3 CNT as a flexible and stretchable sensor material

In addition, CNT film has an ability to bend repeatedly without fracturing so that it provides possibility of high stretchable strain sensor and large strain range detection. If CNT thin film has high stretchability with maintaining good electrical conductivity, tremendous application would be possible in wearable stretchable devices.

However, applications using single nanotube devices, have superior in some aspects, such as in major flaw of irreproducibility. It is difficult to reproduce single tube devices consistently due to the variations in chirality and geometry from tube to tube. However, in a nanotube network, the effects due to such individual variations are suppressed by the ensemble averaging over a large number of tubes.[75] Therefore, NTNs can be reproducibly mass produced, and high efficiency, making them ideal for applications.

The percolated nanotube network, in addition to being flexible and conductive will opening a new application opportunities. The overall conductance is 4 orders of magnitude larger that the resistance of the tube themselves. Reducing the intratube resistance appears to be the primary avenue for increasing device performance. [76]

3.4 Deposition method of CNT for Strain and Pressure Sensor

For the deposition method of CNT in our sensor, spray gun deposition was used to deposit CNT thin films on SMP. Spray gun deposition has already been adopted as a scalable process used to uniformly deposit metallic thin films, such as CNTs.[77,78] The spray gun deposition method is known to be simple, cost-effective and fast. We used a 0.5 mm diameter atomizing nozzle and pressures below 0.5 bar for the deposition of the CNT thin film. The

thickness of the CNT thin film was easily controlled by the number of spray depositions on the substrate.

CHAPTER 4 : Silicon based Elastic Polymer

4.1 Elastic Polymer Substrate for Flexible Wearable Sensors

Another aspect to consider for improving wearable strain and pressure sensor is the careful selection of the flexible and stretchable elastomeric substrate. Polydimethylsiloxane (PDMS) is polymeric organosilicon compounds most widely used silicon-based organic polymer, and is particularly known for its unusual rheological properties. PDMS is optically clear, non-toxic, inert, and non-flammable. Many strain and pressure sensors have been fabricated using polydimethylsiloxane (PDMS) as the stretchable and flexible substrate due to its flexibility, non-toxicity, ease of fabrication, and biocompatibility.[79,80] Amjadi et al. reported highly flexible, stretchable sensitive strain sensors based on silver nanowire with PDMS that had a GF of 14 at 70% strain.[80] For pressure sensor example, Park et al. fabricated polydimethylsiloxane (PDMS)/carbon nanotube (CNT) composite interlocking microdome surfaces achieving pressure sensitivities of up to 15.1 kPa-1.[81] Rough surfaces could also be made by molding silk textile with CNT/PDMS composite materials to achieve pressure sensitivities of up to 1.80 kPa-1.[82]

Speaking about strain sensor, however, many PDMS substrate based strain sensors showed low stretchability with high hysteresis due to poor adhesion between the functional material and substrate polymer, as well as increased friction during the strain.[2,83] The Young's moduli mismatch between PDMS(0.4–3.5 MPa) and the human skin(25–220 kPa) induces more strain into the strain sensor, and even more so when integrated with metallic layers such as CNT, Ag, Au, and Si.[41,79,84–86]

4.2 Ecoflex Substrate

There have been recent efforts to mimic the properties of the human skin more accurately by using Ecoflex, a platinum-catalyzed elastic silicone material. Ecoflex is platinum-catalyzed silicones elastomer that is versatile and easy to use. Ecoflex is mixed 1A:1B by weight or volume and cured at room temperature with negligible shrinkage. Low viscosity ensures easy mixing and de-airing. Cured material is skin safe and certified by an independent laboratory to ISO 10993-10, Biological evaluation of medical devices. Cured Ecoflex is very soft, very strong and very "stretchy", stretching many times its original size without tearing and will rebound to its original form without distortion. Ecoflex has a Young's modulus of ~125kPa, similar to that of human epidermis.[86] Second, it can stretch and withstand strains greater than 900% and rebounds back to its initial size without tearing and distortion. Third, it is highly water resistant allowing for long term wear on the human body. Lastly, Ecoflex is biocompatible, nontoxic, and FDA approved. Therefore Ecoflex is a more suitable candidate for wearable strain sensors.

4.3 PDMS Substrate

In particular, for flexible pressure sensors, it provides electrical feedback in response to external forces including pulsatile blood flow, respiration, and human touch/movement.[8,87] To being robust and conformal, they must be mechanically flexible and stretchable while maintaining high pressure sensitivities and quick response times. Piezoresistive sensors are work by detecting the change in resistance upon actuation. This is typically structured by coupling two conductive rough surfaces together. By doing so, the number of electrical contacts can be changed by the amount of mechanical pressure that is applied, effectively increasing or lowering

resistivity between the electrodes. So, for flexible pressure sensor the substrate has to have both flexibility for conformal and specific stiffness to decrease nose besides from actual external pressure which is applied. So PDMS is more suitable for flexible pressure sensor.

CHAPTER 5 : Highly Flexible Wrinkled Carbon Nanotube Thin Film Strain Sensor to Monitor Human Movement

5.1 Introduction

There is a growing need to improve the mechanical reliability of flexible electronics as the demand for 'wearable' applications in health and medical monitoring increases. These new wearable electrical components must conform to soft curvilinear surfaces, stretch and flex with the body's motion, and be lightweight and unobtrusive. It is critical to overcome rigid, brittle, and largely planar electronics and sensors to develop more insightful investigations for human body monitoring.[1,2] Thus, flexible electronics will fulfill the growing interest in long term monitoring systems for personalized fitness, physical rehabilitation, finger sensing microswitches, entertainment devices, and continuous health monitoring for various parameters such as blood pressure, breathing and body temperature.[3–9]

Wearable strain sensor devices are designed to be mounted on the human skin to measure the strain induced by muscle movements. Many sensors transduce the mechanical deformation to a resistance change upon stretching and releasing. This phenomenon is known as the piezoresistive effect. The relative change in resistance, $\Delta R/R_0$, is related to the mechanical strain ε by the gauge factor (GF) according to Equation (5.1).[1]

$$GF = \frac{\Delta R / R_0}{\varepsilon} \tag{5.1}$$

In order to be an effective strain sensor for monitoring human motion, the sensors must have high flexibility and stretchability, while maintaining sensitivity across a large dynamic

range. For example, high gauge factor strain sensors are able to measure both small and large angle deformations inherent to human joint motion. Thus, there has been a large amount of research in developing highly stretchable and sensitive wearable strain sensors by using micro/nanostructured thin films, functional materials, and elastomeric substrates. Micro- and nanostructures have been implemented by researchers to improve the elasticity of brittle materials.[10–12] These micro/nanostructures are typically generated via buckling from compressive substrates. For example, researchers have deposited brittle materials onto pre-strained silicon rubbers and released the strain to create wavy buckled structures. These wavy buckled structures provided strain relief for brittle materials rendering them stretchable.[13,14]

Typical wearable strain sensors consist of patterned thin films on flexible elastomeric substrates. Recent developments in creating highly stretchable wearable strain sensors used nanoscale metal thin films,[15] nanoparticles,[16] nanowires (NWs),[17–19] nanotubes,[20–26] and graphene.[27–31] For example, Kang et al. utilized brittle platinum thin films to achieve high sensitivity (GF > 2000), but the strain sensor was only able to withstand strains of up to 2%.[32] Li et al. investigated graphene woven fabric for strain sensing (GF ≈ 1000), but was still limited to a maximum strain of 6%.[33] Conversely, Yan et al. reported highly stretchable graphene-nanocellulose nanopaper that can stretch out to 100% strain, but the strain sensor only had a GF of 7.1.[34] Zaretski et al. reported a highly sensitive strain sensor using metallic nanoislands on graphene with GF 1335 at 1% strain. However, the dynamic range of this sensor was limited, with strain of less than 10% strain. Additionally, the GF dropped to 743 after 19 cycles at 1% strain.[88]

Another popular functional material that is used for strain sensing is carbon nanotubes (CNTs). Percolating networks of CNTs on flexible elastomeric substrates have been reported to

have electromechanical stability under high strain due to the robust contact between individual CNTs.[35] CNT thin films have also shown the ability to bend repeatedly without fracturing.[36–40] Therefore, percolating networks of CNTs have the potential to be used as highly stretchable strain sensing devices. For instance, Yamada et al. aligned CNT thin film on PDMS and showed 280% strain but low sensitivity (GF < 0.82),[25] and Lipomi et al. investigated spring like structures in the nanotube that reach 150% strain with good conductivity.[89] Ryu et al. showed that aligned CNT fibers grown on flexible substrates were able to stretch out to 900% having GF of up to 47.[41] However, this process required highly ordered alignment of CNT fibers using intricate dry spinning methods.

Another aspect to consider for improving wearable strain sensor is the careful selection of the stretchable elastomeric substrate. Many strain and pressure sensors have been fabricated using polydimethylsiloxane (PDMS) as the stretchable and flexible substrate due to its flexibility, non-toxicity, ease of fabrication, and biocompatibility.[79,80] Amjadi et al. reported highly flexible, stretchable sensitive strain sensors based on silver nanowire with PDMS that had a GF of 14 at 70% strain.[80] For pressure sensor example, Park et al. fabricated polydimethylsiloxane (PDMS)/carbon nanotube (CNT) composite interlocking microdome surfaces achieving pressure sensitivities of up to 15.1 kPa-1.[81] Rough surfaces could also be made by molding silk textile with CNT/PDMS composite materials to achieve pressure sensitivities of up to 1.80 kPa-1.[82]

Speaking about strain sensor, however, many PDMS substrate based strain sensors showed low stretchability with high hysteresis due to poor adhesion between the functional material and substrate polymer, as well as increased friction during the strain.[2,83] The Young's moduli mismatch between PDMS(0.4–3.5 MPa) and the human skin(25–220 kPa) induces more

strain into the strain sensor, and even more so when integrated with metallic layers such as CNT, Ag, Au, and Si.[41,79,84–86]

There have been recent efforts to mimic the properties of the human skin more accurately by using Ecoflex, a platinum-catalyzed elastic silicone material. Ecoflex has a Young's modulus of ≈125 kPa, similar to that of human epidermis.[90] Second, it can stretch and withstand strains greater than 900% and rebounds back to its initial size without tearing and distortion. Third, it is highly water resistant allowing for long term wear on the human body. Lastly, Ecoflex is biocompatible, nontoxic, and FDA approved. Therefore, Ecoflex is a more suitable candidate for wearable strain sensors.

In this chapter, we introduce a scalable and simple method to fabricate wearable strain sensors with self-similar nano- to microsized wrinkled CNT thin film in Ecoflex. We have previously demonstrated that self-similar hierarchal wrinkled structures in metal thin films can be created via heat induced biaxial shrinking on shape memory polymers (SMPs), such as polystyrene(PS).[91] The buckling occurs due to the mismatches in stiffness between the SMP and the deposited material during the shrinking process.[92] Spray gun deposition was used to deposit CNT thin films on SMP. The spray gun deposition method is known to be simple, cost-effective and fast. Spray gun deposition has already been adopted as a scalable process used to uniformly deposit thin films, such as CNTs.[77,78] Spray gun deposition and the use of SMP makes our fabrication process scalable, simple, and quick compared to other CNT based strain sensors methods. Here we demonstrate that mats of deposited CNTs on the SMP result in densified, self-similar nano- to microfeatured wrinkles upon shrinkage. We show that these wrinkled CNT thin films can be transferred from the rigid SMP carrier film into Ecoflex 0030. (Smooth-On, PA). The tight entangled CNTs introduce strong van der Waals forces between CNTs to enhance

stretchability. Furthermore, these hierarchal self-similar wrinkled structures provide large amounts of strain relief during stretching. To our knowledge, this is the first demonstration of wrinkled CNT thin films fabricated using SMPs, which were integrated in a stretchable human motion sensor.

5.2 Experimental Design

5.2.1. Fabrication of Self-Similar Wrinkled CNT-Ecoflex Strain Sensor

Initially, prestressed PS (KFS50-C, Grafix Arts) was rinsed with ethanol followed by deionized water. The sensor pattern was designed with CAD software (Autodesk, Inc., CA) and patterned on adhesive polymer film (Frisket Film, Grafix Arts). The pattern was subsequently cut with laser cutter (VLS2.30, Universal Laser Systems, AZ) and placed patterned adhesive polymer film, as a shadow mask, on top of a PS substrate. Spray gun method is used for deposit CNT solution (Aldrich) to the masked PS substrate. For the spray gun, the atomize nozzle and 0.5 mm tip size is used, the pressure was kept below 0.5 bar and the distance between spray gun and masked PS substrate is 25 cm for uniformity of CNT thin film deposition. The dispersed fluid of CNT solution, was evaporated by heating on the hotplate (≈65 °C) while spray gunned. The thickness of the CNT thin film is 115 nm and could be controlled by the amounts of the spray gunned CNT solution and distance between the spray gun and the working substrate. The thickness of CNT will affect to the size and wavelength of wrinkles which will affect its stretchability. The patterned CNT thin film was rinsed with deionized water for 10 min to remove surfactant and organic residue and dried completely with N_2 gun and light heating. After

removing of the patterned shadow mask film, the deposited CNT thin film was pressed by the roller. The sample was placed into a convection oven for heat approximately to 150 °C to induce biaxial shrinking and wrinkling into the CNT thin film. The sensor design was shrunk to 33% of initial size. After forming a self-similar wrinkle on CNT thin film, a platinum-catalyzed silicone elastomer (Ecoflex 0030, Smooth-On, PA) was poured and spin coated (Laurell Technologies Corporation) at 150 rpm for 40 s. After spin coating, shrunk sample was placed under vacuum for 10 min to remove bubbles and cured overnight at room temperature. Cured sample was placed into an acetone bath (75 °C) for 30 min followed by a toluene bath (65 °C) 10 min to remove any residual PS then dry in air for 12 h.

5.2.2. Structure Characterization and Sensing of Strain

SEM (FEI Magellan 400 XHR) was performed for imaging the wrinkles, and CNTs. The samples were sputter coated with Ir prior to SEM imaging. Strain sensitivity of wrinkled CNT-Ecoflex sensors was measured by a custom-made semi-static tensile strain stretching apparatus. The apparatus was a leadscrew based linear actuator driven by a stepper motor (Figure 3a). To avoid mechanical failure and to withstand large deformations while maintaining high electrical conductivities, liquid metals such as eutectic gallium-indium (EGaIn) were used rather than solid materials. Sensor is fixed at 0% strain and resistance is measured by 30% strain increments until failure. For cycling measurement, the sensors where strained from 0% to 300% using a sawtooth wave form on a computer controlled linear strain testing apparatus. The resistance was sampled at 2 Hz with a multimeter connected to a computer. The samples were cycled over 1000 times at 2 Hz.

5.2.3. Detecting the Human Motion (Finger, Elbow, and Knee)

The wrinkled CNT-Ecoflex sensor was assembled on an elastic sports fitness tape to hold all the components together (Figure 6c inset). Measurements were taken using the same data acquisition system as previously mentioned. Finite Element Analysis: FEA was performed to examine the strain and stress distribution in the Ecoflex and CNT film respectively. The models were created using Ansys DesignModeler, and analysis was performed with Ansys Workbench 16.0. The Ecoflex was modeled as a two parameter Mooney-Rivlin hyperleastic material,[93] and the carbon nanotube film was modeled as an isotropic elastic material. The stiffness of the carbon nanotube film was calculated using the wrinkle wavelength equation used by Fu et al.[94] To examine the distribution of normal stress within the carbon nanotube film, a simplified 2D model was created based off of SEM cross-section images of the of the transferred carbon nanotube sensor. The model was strained to 300% strain. To assess the normal strain distribution within the Ecoflex, three different Ecoflex geometries (rectangular, dumbbell, and hourglass) were modeled; each geometry was taken to 425% strain.

5.3 Results and Discussion

5.3.1 Fabrication of Strain Sensor

The fabrication process for self-similar wrinkled CNT-Ecoflex (wCE) strain sensors can be seen in **Figure 5.1.** A spray gun was used to deposit CNTs through a shadow mask and onto a

PS substrate. We used a 0.5 mm diameter atomizing nozzle and pressures below 0.5 bar for the deposition of the CNT thin film.

The thickness of the CNT thin film was easily controlled by the number of spray depositions on the substrate. After the spray deposition, the patterned CNT thin film was rinsed with deionized water and dried. After removing the patterned shadow mask, a paint roller was used to press against the CNT thin film to make the thin film denser. This step was performed to

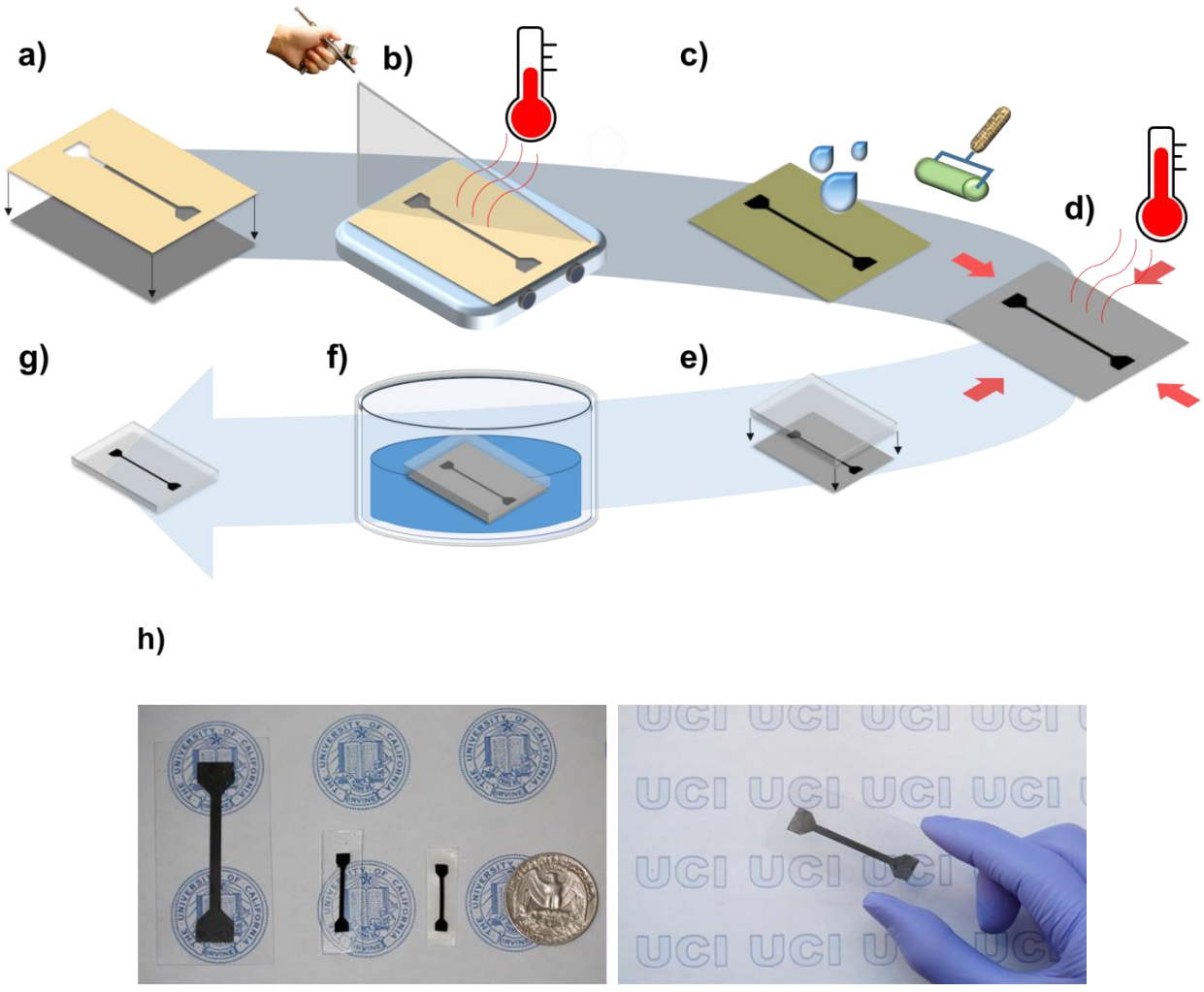

Figure 5.1. Fabrication process of self-similar wrinkles CNT-Ecoflex strain sensor. a) Shadow mask is attached onto PS substrate b) Spray gun is used to deposit CNT thin film. c) Substrate was rinsed with deionized water and applied with pressure from a roller. d) Heat was applied to

induce biaxial shrinking e) Ecoflex was cured on shrunken PS substrate. f) Organic solvent bath was used to complete transfer process. g) Final self-similar wrinkled CNT thin film on Ecoflex substrate. h) Photograph of the CNT thin film at each step of the fabrication process: As deposit, shrunken, transferred (left) and CNT thin film on PS substrate (right).

---

prevent the CNT network from embedding into the PS during heat induced shrinking. The sample was then placed into a convection oven set at 150 °C to induce biaxial shrinking and wrinkling of the CNT thin film. After shrinking, the sensor is about 33%–40% of the original size. After shrinking, Ecoflex was spun on top the sample and cured overnight at room temperature. The cured sample was then placed into an acetone bath followed by a toluene bath to transfer the wrinkled CNT thin film onto Ecoflex. **Figure 5.2** shows scanning electron microscope images of the CNT thin film at different stages of the fabrication process. As deposited planar CNT thin film on PS is shown in **Figure 5.2a**. After heat induced shrinkage, the CNT thin film buckled and created self-similar wrinkled structures similar to those previously shown in metal thin films.[95] The CNT thin films wrinkle because each individual CNT is entangled and weakly adhered to each other via van der Waal forces resulting in one thin film as opposed to an assortment of individual CNTs. Scanning electron microscopy (SEM) images in the right-hand column of **Figure 5.2** show that these wrinkled structures are comprised of individual CNTs. As seen in **Figure 5.2c**, the wrinkled structures were maintained after transferring into the soft silicone elastomer, Ecoflex. However, the shape of the wrinkles slightly changed due to swelling and shrinking of the Ecoflex during the organic solvent transfer process. The overall shape of the self-similar wrinkled structures was maintained. These selfsimilar wrinkled structures supported by a soft silicone elastomer allow the CNT thin film to become highly elastic.

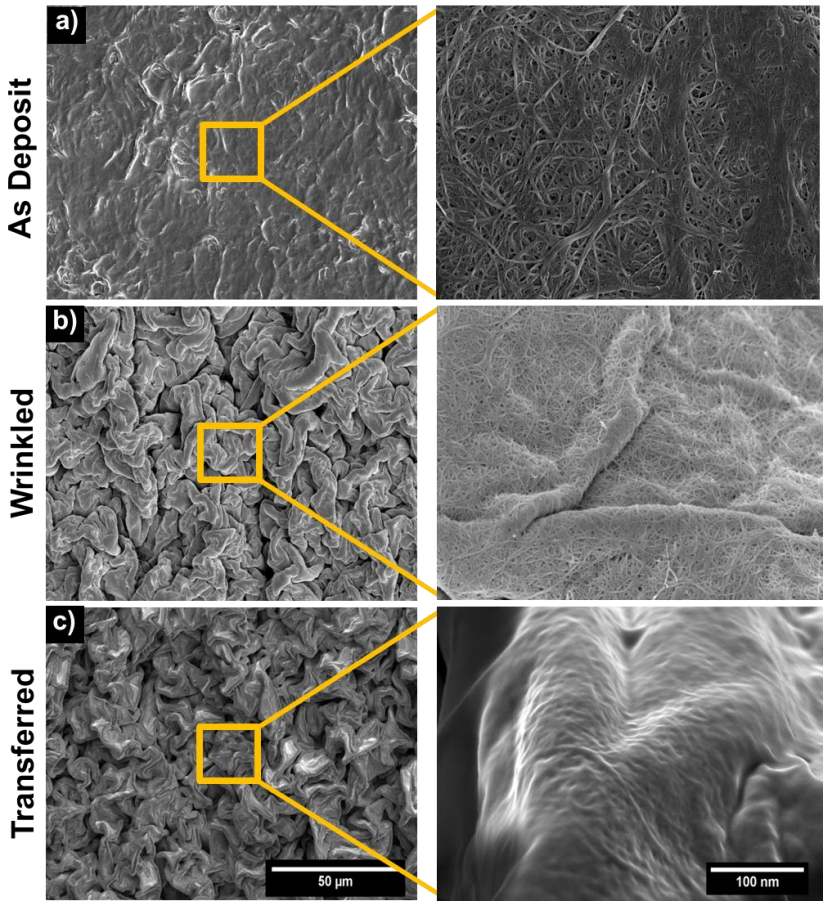

Figure 5.2. Scanning electron microscope images of the wrinkled CNTs. a) As deposited CNT thin film on PS substrate. b) Wrinkled CNT thin film on shrunken PS substrate. c) Transferred wrinkled CNT thin film on Ecoflex substrate.

5.3.2 Mechanism of Wrinkled Structures

Figure 5.3 shows the stretching apparatus for straining and the strain-resistance behavior of self-similar wrinkled CNT thin films. As seen in **Figure 5.3**, wCE strain sensors were able strain CNT thin films (the control) were only able to stretch out to ≈12% (**Figure 5.4**). Therefore, the wrinkled structures provided a > 60 fold increase in stretchability. The reproducibility for the strain resistance behavior is shown in **Figure 5.5**

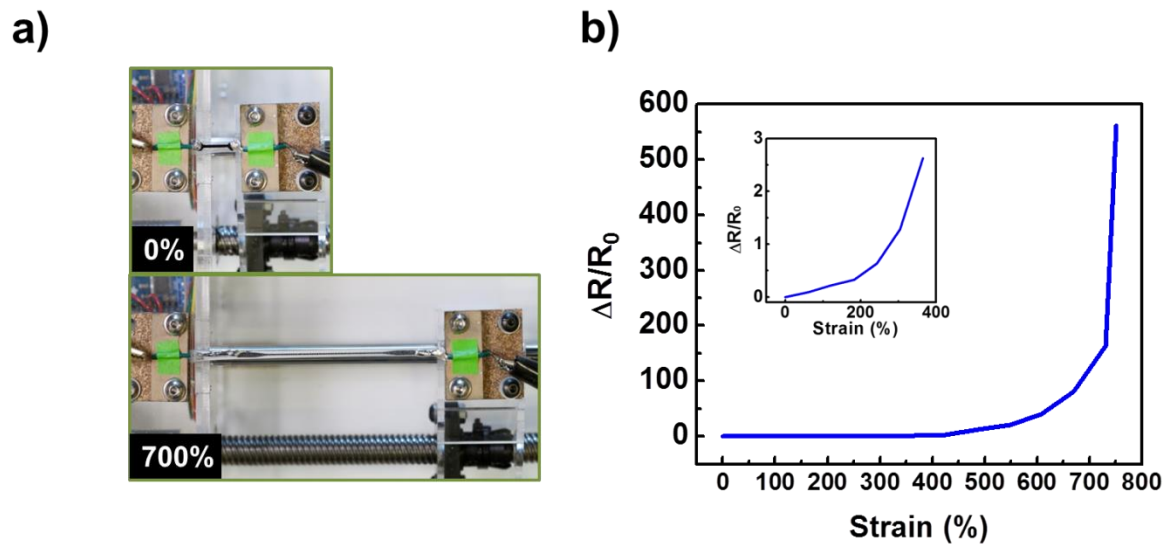

Figure 5.3. a) Image of a strain sensor at the initial length and stretched to 700% strain. b) Relative change in resistance vs strain on wrinkled CNTs on Ecoflex substrate. (the inset plot is expanded view of 0-400% strain)

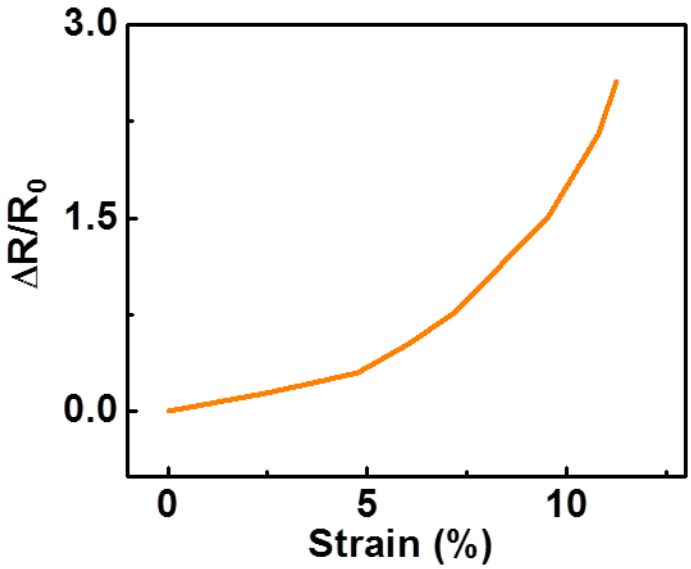

Figure 5.4. Relative change in resistance vs strain for as deposited planar CNT thin film.

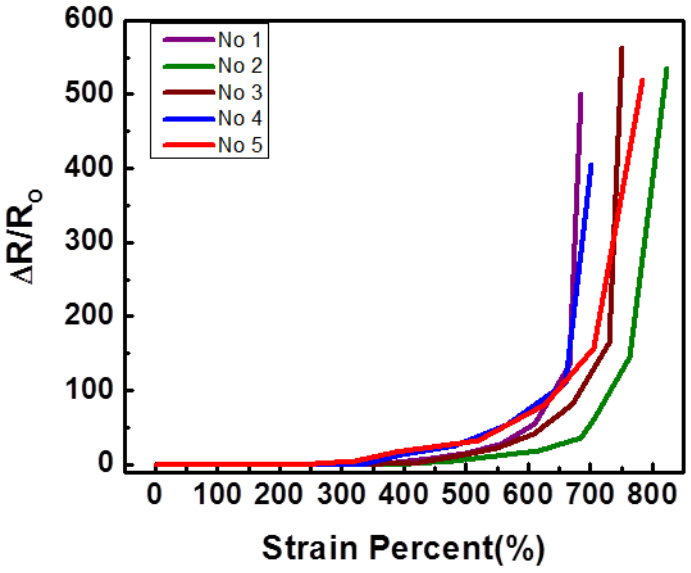

Figure 5.5. Relative change in resistance vs strain on multiple wCE strain sensors.

The strain-resistance plot shows two distinct regions of strain: 0%–400% and 400%–700%. In the first region from 0%–400% strain, the relative change in resistance increased by a factor of 2.5 and the GF was 0.65. For this region, the change in electrical resistance is a combination of different factors. Predominantly, it is due to the increasing separation of neighboring wrinkled CNT structures and from the increase in the length of the wrinkle's geometry when stretched. Additionally, there is also a decrease in the effective cross-section area between CNTs and a separation of the individual CNTs by a van der Waals separation distance. This distance change between neighboring CNTs promotes an increase in the tunneling resistance. There may also be deformation of the individual CNTs themselves, which will increases the resistance of the tubes.[10,57–60] The second region from strains 400%–700%, the relative change in resistance increased by a factor of 162 and had a GF of 48. In this region, the CNT thin film started to fracture at strains greater than 400% as evidenced from the discontinuities and gaps within the thin film (**Figure 5.6**). This reduces the number of conductive pathway so the relative change in resistance very large. Finite Element Analysis (FEA) of a 2D cross section show that the normal stress is localized within the valleys of the wrinkles during strain. Furthermore, within each valley, the normal stress is highest at the top of the CNT thin film, CNT-Air interface, and lowest at the CNT-Ecoflex interface (**Figure 5.7**).[85] As the model suggests, these localized stress points are most likely where the fractures nucleate. Within each valley, the fractures will propagate downward toward the CNT-Ecoflex interface. Throughout the entire film, these fractures expand to form a mesh like pattern of conductive pathways, similar to that of metal thin films.[96] The reduction of conductive pathways results in high resistance changes and subsequent high sensitivity in the second region

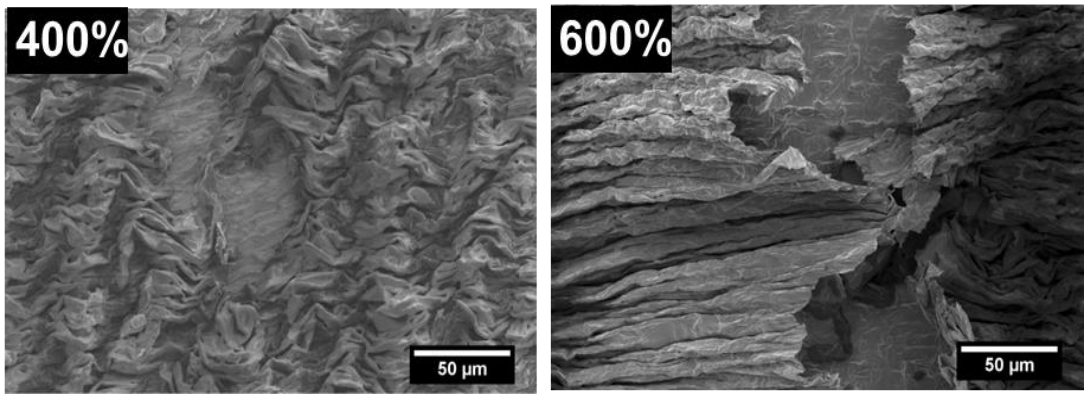

Figure 5.6. Scanning electron microscope images of the wrinkled CNT thin film fractures on Ecoflex at 400% and 600% strain.

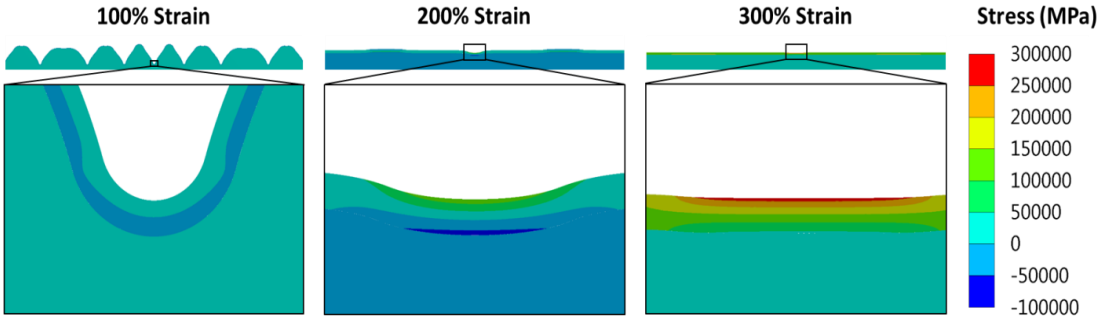

Figure 5.7. Normal stress distribution at 100%, 200% and 300% strains on wrinkled CNTs thin film.

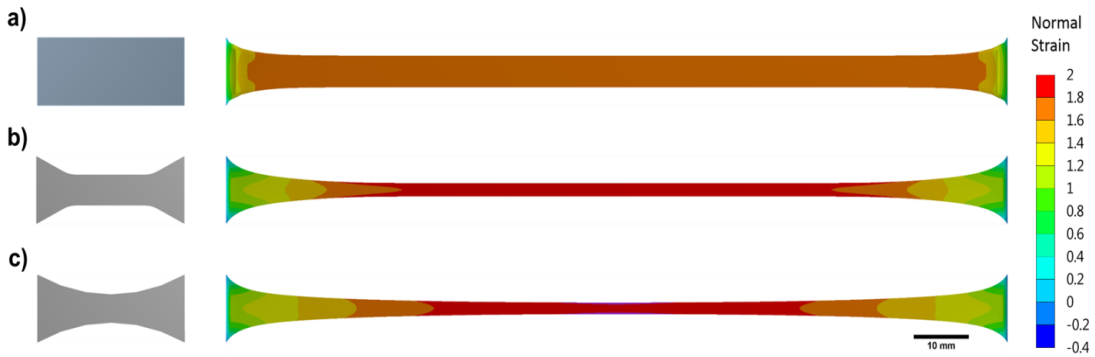

Figure 5.8. Normal strain distribution at 425% strain of three different Ecoflex sensor geometries: a) rectangular b) dumbbell c) hour glass.

The geometry of the elastomeric substrates also affects the performance of the wCE strain sensors. FEA of three different geometries (rectangular, dumbbell, and hourglass) shows that the shape affects the strain distribution throughout the Ecoflex during stretching. (**Figure 5.8**) The FEA of the rectangular shaped elastomeric substrates showed the most uniform strain distribution, while the dumbbell and hourglass shaped geometries showed more localized strain in the center. This nonuniformity may result in earlier fracturing of the sensor in areas of higher strain concentration. Therefore, the rectangular geometry was chosen for the sensor because it maintains uniform strain along the longitudinal direction of the sensor. The uniform strain should help increase strain by uniformly distributing the fracture that occurs, minimizing the chance for a large discontinuity to form.

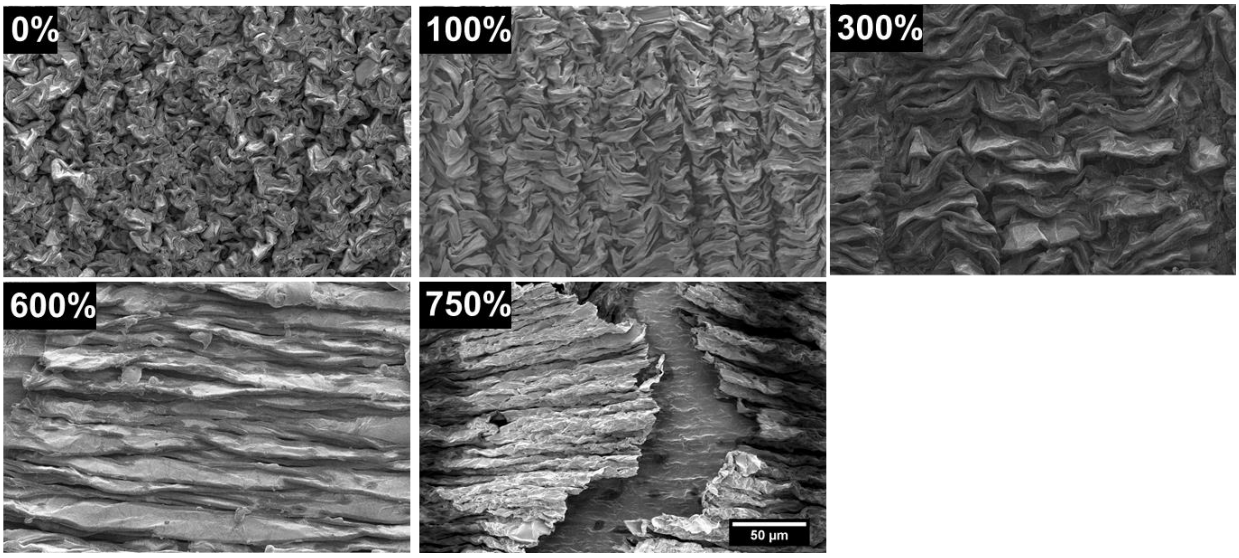

Figure 5.9. Scanning electron microscope images of the wrinkled CNT thin film on Ecoflex at different strains.

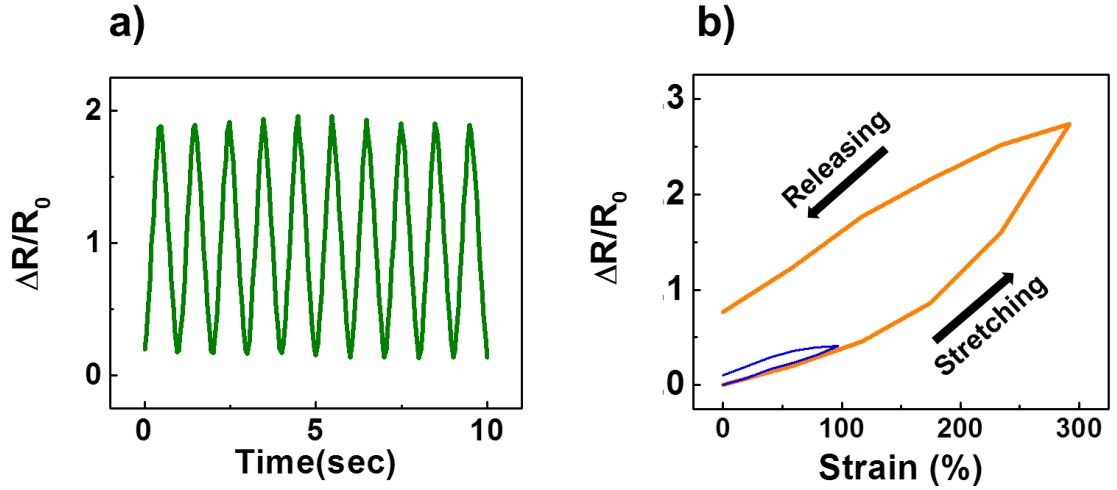

Figure 5.10. a) Relative change in resistance for cyclic strains between 0% and 300%. b) Hysteresis at 100% (blue) and 300% (orange) strains.

Figure 5.9. illustrates how incremental tensile strains, up to 750%, affect the CNT wrinkled structures. At 100% of strain, the CNT wrinkles started to align in the direction of the load. This is due to the compressive strains from the Ecoflex, which follows a positive Poisson ratio. The wrinkle structures completely aligned uniaxially at strains greater than 400%. After this point, the wrinkled structures were not able to provide any more strain relief resulting in fracture nucleation and propagation. Although the wrinkles were completely aligned, additional strain relief came from the percolating network of CNTs. At 750% strain, the fractures propagated completely across the trace resulting in sensor failure.

The response of the wCE strain sensor during a 300% cyclic strain can be seen in **Figure 5.10.** The normalized change in resistance was approximately 175% which corresponds well with **Figure 5.3b**. At 300% strain there was 145% change in resistance similar to that of the cyclic strain. This shows that the wCE sensor were robust after cyclic strain. Cyclic strains of 300% and 500% strain for 1000 cycles are shown in **Figures 5.11** and **5.12** (Supporting Information). In addition to cyclic strain, the hysteresis responses for the wrinkled CNT-Ecoflex strain sensors at 100% and 300% strain were measured (**Figure 5.3b**). After releasing from 100% strain, there was a slight hysteresis showing a 1% change of resistance. Releasing at 300% strain, there was a 7% change of resistance due to the viscoelastic properties of the Ecoflex substrate.

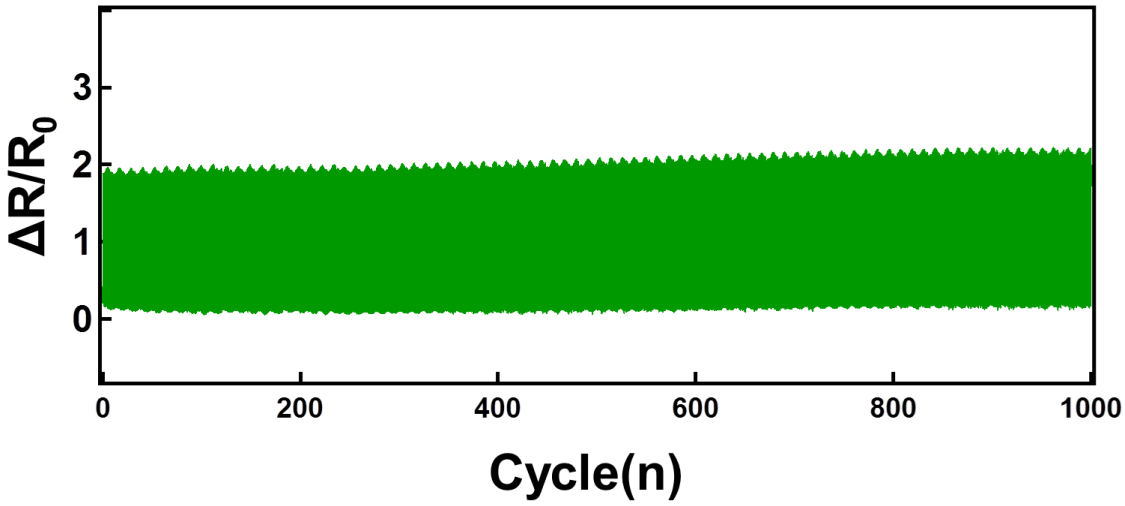

Figure 5.11. Relative change in resistance for cyclic strains between 0% and 300% for 1000 cycles

---

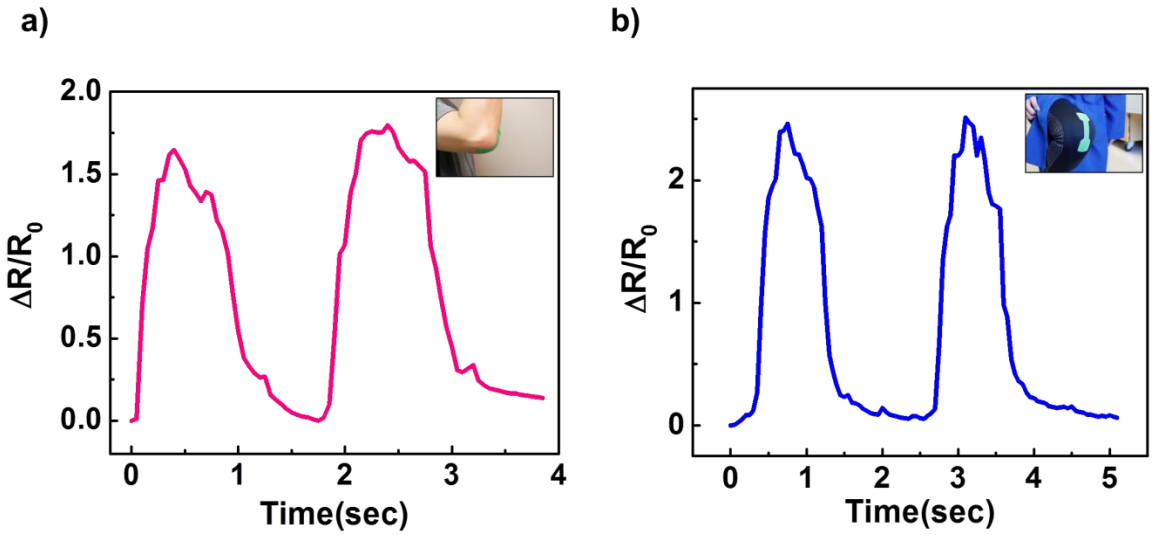

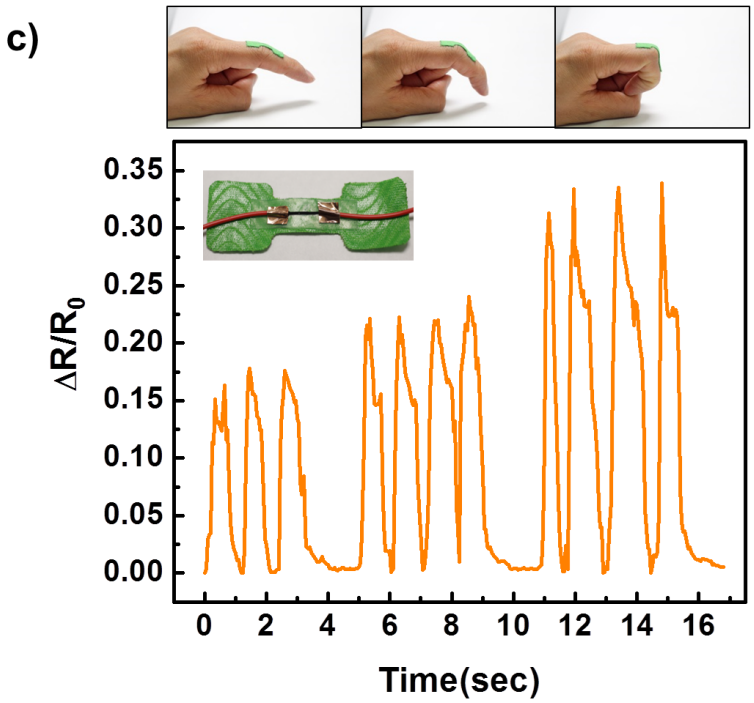

Figure 5.12. Wrinkled CNT-Ecoflex strain sensor was used to monitor human movement. Relative change in resistance while bending the strain sensor at joint area of a) elbow, b) knee and c) finger.

5.3.3 Detecting Human Movements

To demonstrate the potential and applicability of the wCE sensor as a wearable device, the strain sensor was mounted on the elbow, knee, and finger to monitor their motion. The wCE sensor was assembled on an elastic sports fitness tape, KT Tape (KT Health (**Figure 5.12**c inset)). The wCE sensor was attached on the respective joints for the elbow, knee, and finger. (**Figure 5.12**). To measure the movement of the elbow, the initial elbow position was held flat and measurements were taken while the elbow was bent toward the body and returned back to the initial position. During the bending motion, the wCE sensor stretched and bent with the joint

causing the relative change in resistance to increase. When returned back to the original position, the relative change of resistance returned back to baseline. The maximum strain for the elbow bending was 180%. To measure the bending motion of the knee, the sensor was attached on the knee cap and measurements were taken for a squatting motion. The knee was initially straight and then bent during the squatting motion. With a squat position, the sensor bended and stretched, and its relative change of resistance increased up to 230% strain. When returning back to the original position, relative resistance again decreased with the releasing of sensor. Lastly, measurements were made on the middle joint of the index finger at successive bending of 30°, 60°, and 90° (**Figure 5.12c**). The relatively change in resistance increased with increased bending and stretching. The measured relative changes in resistance were ≈17%, 24%, and 33%, respectively. The abovementioned experiments highlight the potential use of CNT–Ecoflex nanocomposite based strain sensors as an epidermal device for human skin motion detection.

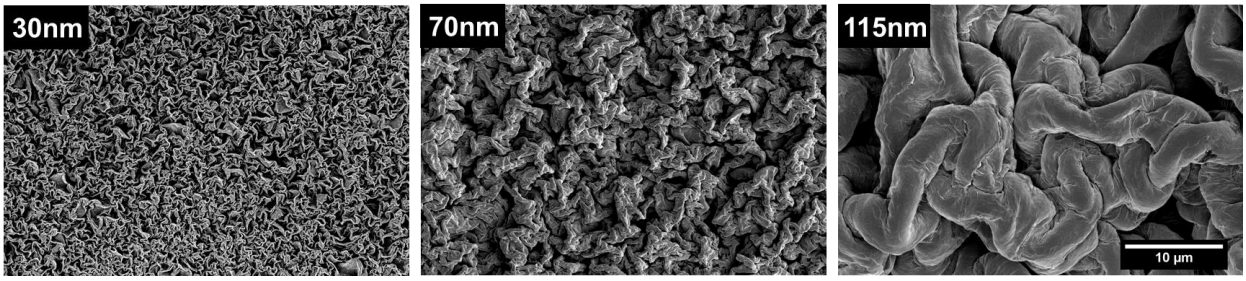

Figure 5.13. Scanning electron microscope images of the wrinkled CNTs thin film on PS substrate at different thicknesses.

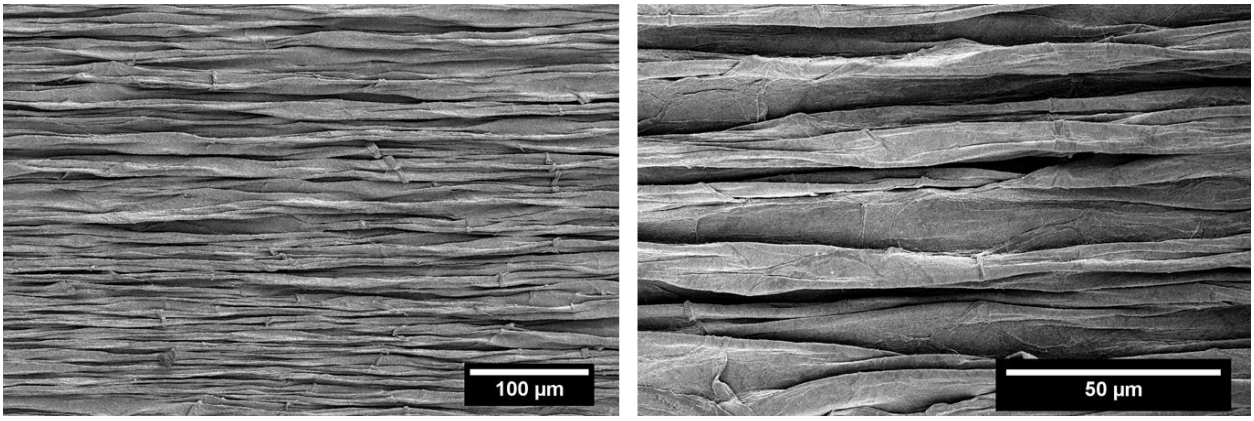

Figure 5.14. Scanning electron microscope images of wrinkled CNT thin film generated from uniaxially heat induced shrinking.

5.4. Conclusion

In conclusion, we have introduced a new route to develop ultra-stretchable, human skin mountable, and sensitive strain sensor with low cost and simple fabrication procedure by forming stretchable wrinkled CNT networks. We have also demonstrated that wrinkled CNT networks can be transferred onto soft stretchable elastomeric substrates such as Ecoflex, while maintaining the self-similar nano- and microstructures and conductivity. Different sizes and wavelengths of wrinkles can be produced by depositing different thicknesses of the CNT solution. The feature size of the CNT wrinkle increases with the film thickness (**Figure 5.13**). Furthermore, by uniaxial shrinking, the CNT wrinkle waves can alternatively align into one direction (**Figure 5.15**). Our fabrication method is compatible with conventional and scalable manufacturing methods as previously reported.[92,97] The wCE sensor can measure up to ≈750% strain with high sensitivity. Finally, we demonstrate the application of the sensors for detecting human motion by mounting the sensors onto the joint areas of the finger, elbow and knee. The maximum strain

measured was ≈300%. This study suggests that these wCE sensors have applicability in a wide application range where measurements of large strains are required for physiological monitoring

Chapter 6 : Flexible Piezoresistive Pressure Sensor Using Wrinkled Carbon Nanotube Thin Films for Human Physiological Signals

6.1 Introduction

Highly flexible, stretchable wearable sensors have received considerable attention due to potential applications for artificial robotic skins[22,98–100], advanced prosthetics[8,46,101,102], and continuous health monitoring applications.[8,84,103,104] In particular, flexible pressure sensors provide electrical feedback in response to external forces including pulsatile blood flow, respiration, and human touch/movement.[8,87,105] Wearable pressure sensors may directly impact continuous health monitoring applications allowing for true and real-time point of care solutions. However, in order for these wearable sensors to be fully realized, several parameters still need to be improved. In addition to being robust and unobstrusive, they must be mechanically flexible and stretchable while maintaining high pressure sensitivities and quick response times. Much effort to date have been directed towards developing novel materials and design configurations to improve mechanical robustness and performance in wearable sensors.[95,106,107] Researchers have reported various transduction mechanisms to detect physical pressure changes including: piezoelectric[11,87,108–110], capacitance[22,100,111–113], and piezoresistive[8,46,114–119]. Each of these transduction mechanisms has its own attributes with particular advantages over the other.

Piezoelectric materials are materials that can produce electrical charges when induced with mechanical stress and have been widely used in pressure sensors.[120] For example, Xiaoliang et al. reported vertically aligned piezoelectric P(VDF-TrFE) nanowires that were able to detect blood pulse on the wrist.[87] The device was able to output a maximum of 4.8V with a

current density of 0.11 μA cm^{-2}. These sensors had high response times and limits of detection of less than 2 Pa, but could only provide dynamic information which greatly limits its applications.

Capacitive pressure sensors consist of a compliant dielectric layer sandwiched by two parallel conductive electrodes. When a pressure is applied, the dielectric layer gets compressed generating an increase in capacitance. Capacitive pressure sensors have been characterized with high signal linearity, but have low pressure sensitivities. Xiaoli et al. reported a flexible capacitive array pressure sensor with a pressure sensitivity of 1.45 MPa^{-1}.[100] Yao et al. have demonstrated that silver nanowires can also be used to fabricate stretchable conductors allowing for pressure sensitivities of up to 1.62 MPa^{-1}.[121] Zang et al. have also demonstrated that compressible dielectric layers can also be incorporated into organic thin-film transistors (OTFTs) achieving pressure sensitivities of up to 192 kPa^{-1}.[122] While high sensitivities were achieved, the device required high voltages to achieve high sensitivities (V_{ds} = -60 V). Although capacitive pressure sensors exhibit highly linear signal responses, they are generally characterized with poor sensitivity due to the small compression of the dielectric layer. Higher sensitivities can only be achieved by using higher voltage sources.

Piezoresistive sensors work by detecting the change in resistance upon actuation. This is typically structured by coupling two conductive rough surfaces together. By doing so, the number of electrical contacts can be changed by the amount of mechanical pressure that is applied, effectively increasing or lowering resistivity between the electrodes. For example, Park et al. fabricated polydimethylsiloxane (PDMS)/carbon nanotube (CNT) composite interlocking microdome surfaces achieving pressure sensitivities of up to 15.1 kPa^{-1}.[123] Rough surfaces could also be made by molding silk textile with CNT/PDMS composite materials to achieve pressure sensitivities of up to 1.80 kPa^{-1}.[124] Silver nanowire (AgNW) networks have also been

demonstrated to have pressure sensitivities of up to 5.8 kPa^{-1} due to the bridging effect between each of the particles.[125] Wang et al. reported piezoresistive pressure sensors using microhump structures with pressure sensitivities of 851 kPa^{-1} and response times of 0.15ms.[117] When pressure was applied, the number of electrical contacts increased allowing for higher current to flow between the conductive surfaces. However the conformability was limited, and it had a high detection limits of 34 Pa. For a more thorough review of pressure sensors, please see following reference.[126]

Here we report highly structured and elastic carbon nanotube thin films as rough conductive electrodes for piezoresistive pressure sensing. Previously, we reported wrinkled carbon nanotube (wCNT) strain sensors that were able to withstand strains of up to 700% before electrical failure.[127] Using the same shrinking fabrication process, highly wrinkled carbon nanotube thin film electrodes were coupled face-to-face to produce piezoresistive pressure sensors. By incorporating highly wrinkled structures into CNT thin films, pressure sensitivities were improved 12800 fold.

6.2. Experimental Design

6.2.1 Synthesis of Carbon Nanotube Solution

SWCNTs (>80 wt%) were obtained from Sigma-Aldrich. SWCNTs (1 mg mL^{-1}) were dispersed in an aqueous solution of sodium dodecyl sulfate (10 mg mL^{-1})(Bio-Rad Laboratories) by ultrasonication for 4hrs in an ice bath. The dispersed SWCNT solution was then centrifuged at 12,000 rpm for 70min in a fixed-angle rotor (Fiberlite F15-8x50cy, Thermo Scientific) to

remove the residue of catalytic metal particles. The upper 90% of the supernatant was collected and used for deposition.

6.2.2 Fabrication of Nanowrinkled CNT-PDMS Pressure Sensor

Pre-stressed polystyrene (PS) (KFS50-C, Grafix Arts) was rinsed with 70% ethanol and dried with N_2. The square sensor electrode (1.5 inch x 1.5 inch) was designed with CAD software (Autodesk, Inc., CA) and patterned on adhesive polymer film (Frisket Film, Grafix Arts). The square pattern on adhesive polymer film was cut using a laser cutter (VLS2.30, Universal Laser Systems, AZ) and placed on top of a PS substrate as a shadow mask. A spray gun wasused to deposit synthesized CNT solution to the masked PS substrate. During the spray gun deposition, a 0.5mm nozzle size, 0.5 bar pressure, and a 25 cm distance from the masked PS substrate were used. to ensure a continuous, and uniform CNT thin film (~80nm). The masked PS substrate was heated on a hotplate at (≈70^{o}C) to ensure evaporation of the CNT solution as it was deposited. The deposited CNT thin film was rinsed with deionized water to remove surfactant. After removing the shadow mask, the PS was then heated to approximately 150 °C to induce shrinking causing the CNT thin film to buckle and form highly wrinkled structures. Biaxial shrinking allows up to each axis to shrink up to 40% of its original length. To induce uniaxial shrinking, two ends of the PS substrate were clamped with binder clips to prevent one axis from shrinking. After shrinking, a silicone elastomeric polymer, polydimethylsiloxane (PDMS, Dow Corning Sylgard 184) was used to spin cast a 1 mm thick layer on the PS substrate. Cured sample was then placed into an acetone bath (75 °C) followed by a toluene bath (65 °C) to remove any residual PS. Silver paste was used to make interconnects to the wrinkled CNT

electrodes. The wrinkled CNT-PDMS films were then placed face-to-face and sealed with Kapton tape.

6.2.3 Structure Characterization

The wrinkled structures of the CNT thin film was characterized using scanning electron microscope(SEM, FEI Magellan 400 XHR). The samples were sputter coated with Ir (5nm) prior to SEM imaging.

6.2.4 Pressure Sensitivity & Cycling

The relative change in resistance of the wrinkled CNT-PDMS sensor under applied force was measured using a force gauge (Series 5, Mark-10).and an LCR meter (E4980A, Keysight Tech.) using the 4 point probe method at 1V.

6.2.5 Detecting the Human Physiological Signals (Pulsatile blood flow, Voice detection)

The wrinkled CNT-PDMS pressure sensor was assembled on an elastic sports fitness tape to hold all the components together. Measurements were taken using the same data acquisition system as previously mentioned.

6.2.6 Finite Element Analysis

FEA was performed on simplified geometries of the 1D and 2D wrinkles using Ansys workbench 16.0. The 2D wrinkles were modeled with a radius of 3.5 um, height of 4 um, and wavelength of 8 um; while 1D wrinkles had a radius of 2 um, height of 8.5 um, and wavelength of 5 um. The material property was assumed to be PDMS, and three different combination of wrinkle morphologies were modeled: 1D-1D contact, 2D-2D contact, and 1D-2D contact. The degree of contact was determined by the number of nodes touching between each surface as displacement was increased. Contact was recorded over time and normalized to the initial value such that the initial number of nodes touching is equal to 1.

6.3. Results and Discussion

6.3.1 Fabrication of Pressure Sensor

The detailed fabrication process is described in the Experimental Section. As shown in **Figure 6.1**, a CNT thin film was deposited onto a polystyrene (PS) substrate using a spray gun deposition method. PS is a shape memory polymer that is able to shrink (~67% in area) back to its original shape when induced with an external stimulus such as heat.[95,127–129] When the PS was heated pass its glass transition temperature (100^{o}C), the PS shrunk causing the CNT thin film to buckle and form highly self-similar wrinkled structures. The buckling formed due to the percolating network nature of the CNT thin film. Each individual CNT was entangled and weakly adhered to each other via van der Waals forces creating a confluent thin film. The entanglement of the percolating network allowed for greater elasticity in the wrinkled CNT thin film as previously shown.[127]

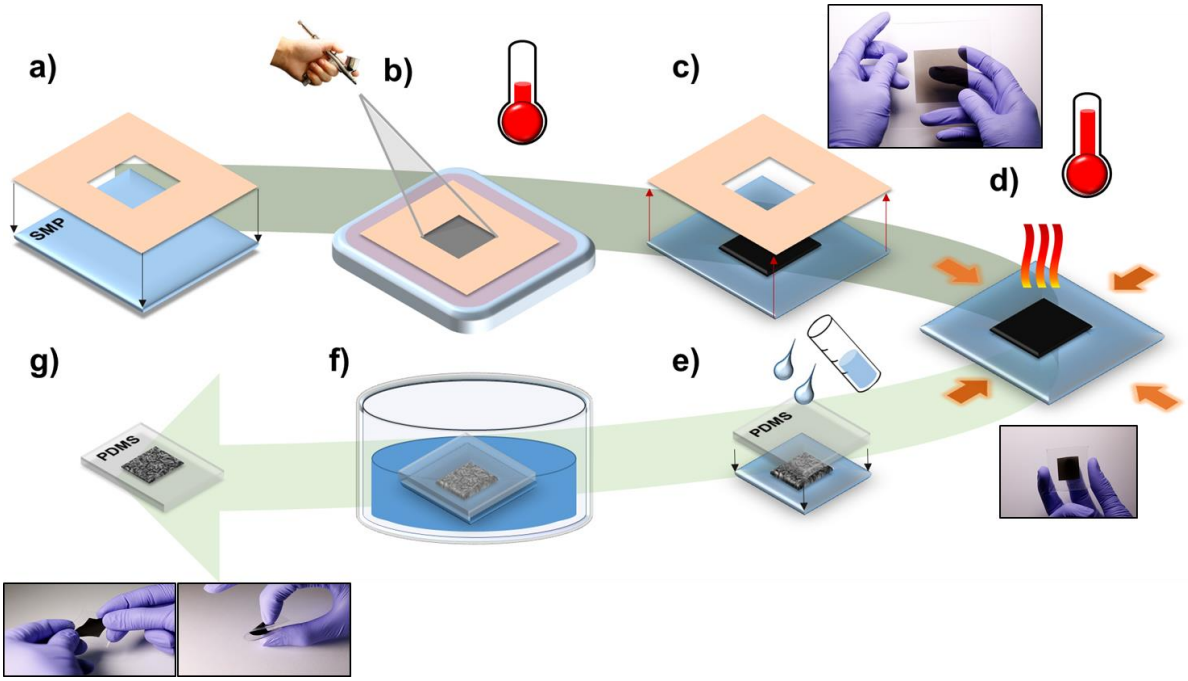

Figure 6.1. Fabrication process flow of wrinkled CNT piezoresistive pressure sensors. a) Shadow mask is mounted onto shape memory polymer (SMP). b) CNT solution is deposited using a spray deposition. c) Shadow mask is removed from SMP substrate. d) SMP substrate was heated to induce biaxial shrinking. e) Polydimethylsiloxane (PDMS) was cured over the SMP substrate. f) Organic solvents were used to transfer the wrinkled CNT thin film onto the PDMS substrate. g) Final wrinkled CNT electrode for piezoresistive pressure sensing.

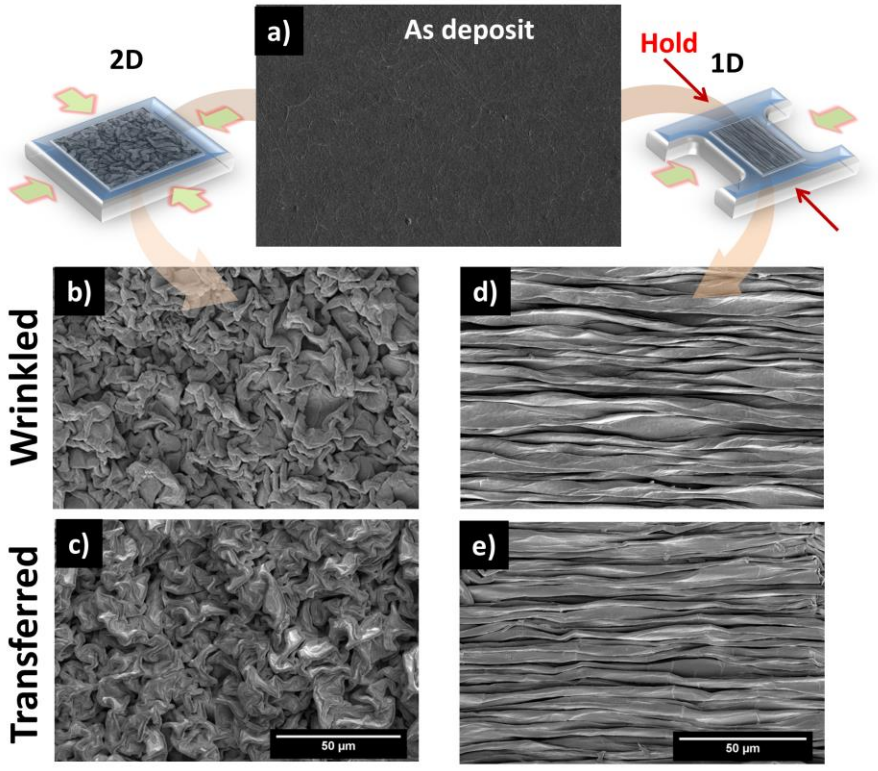

Figure 6.2. Scanning electron microscope images illustrating wrinkled topography. a) CNT thin film deposited on PS substrate b) Biaxially shrunk CNT thin film. c) Biaxially shrunk CNT thin film transferred onto PDMS. d) Uniaxially shrunk CNT thin film. e) Uniaxially CNT thin film transferred onto PDMS

Scanning electron microscope (SEM) images of the CNT thin film can be seen in **Figure 6.2**. **Figure 6.2a** illustrates as deposited CNT thin film on a PS substrate. After thermally induced shrinkage, the CNT thin film buckled and formed self-similar biaxial(2D) wrinkled structures as seen in Figure 2b. To induce uniaxial shrinking(1D), two ends of the PS substrate were clamped down prior to shrinking. The PS substrate will not extend back to its original shape at room temperature. In order for the PS to extend back to its original shape, the PS

substrate needs to be heated past its glass transition temperature again, mechanically stretched to its desired geometry, and cooled to room temperature.

Consequently, this produced uniaxial wrinkles(1D) as seen in **Figure 6.2d**. The wrinkled CNT thin film was then transferred onto a polydimethylsiloxane (PDMS) substrate using an organic solvent transfer process as seen in **Figure 6.2(c,e)**. The morphology of the wrinkled structures slightly changed during this transfer process due to the swelling of the polymer in the organic solvent bath. However, the overall shape was maintained throughout the process. SEM images illustrating the cross sections of the 2D and 1D wrinkled CNTs transferred on PDMS can be seen in **Figure 6.3**

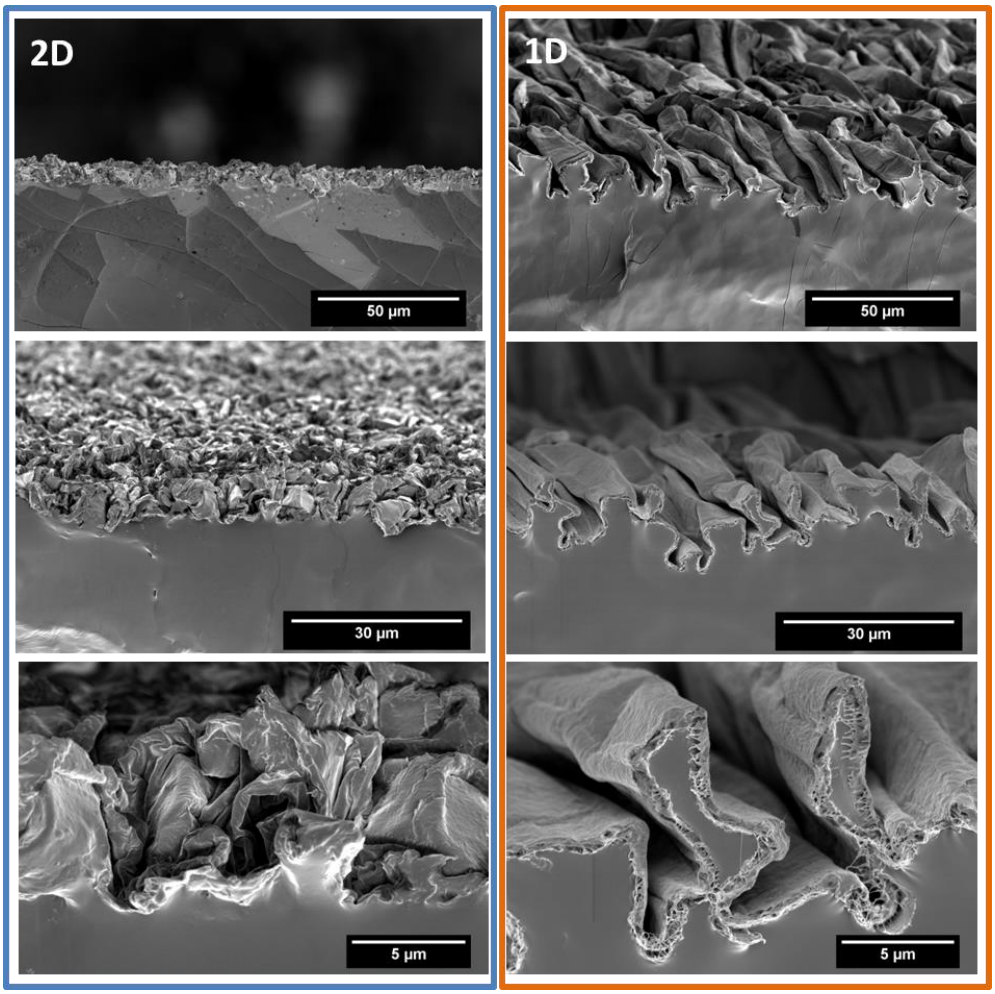

Figure 6.3. Cross sectional scanning electron microscope images of 2D(biaxial, blue column) and 1D(uniaxial, orange column) wrinkled CNT transferred on PDMS.

6.3.2 Measurements of Wrinkled CNT Pressure Sensor

Contact piezoresistive pressure sensors operate by decreasing the electrical resistance between two electrodes by increasing the number of contact points. The pressure sensitivity S of a device is characterized with the following equation:

$$S = \frac{\Delta R / R_0}{\Delta P} \tag{6.1}$$

where R is the resistance, R_o is the initial resistance, and P is pressure.

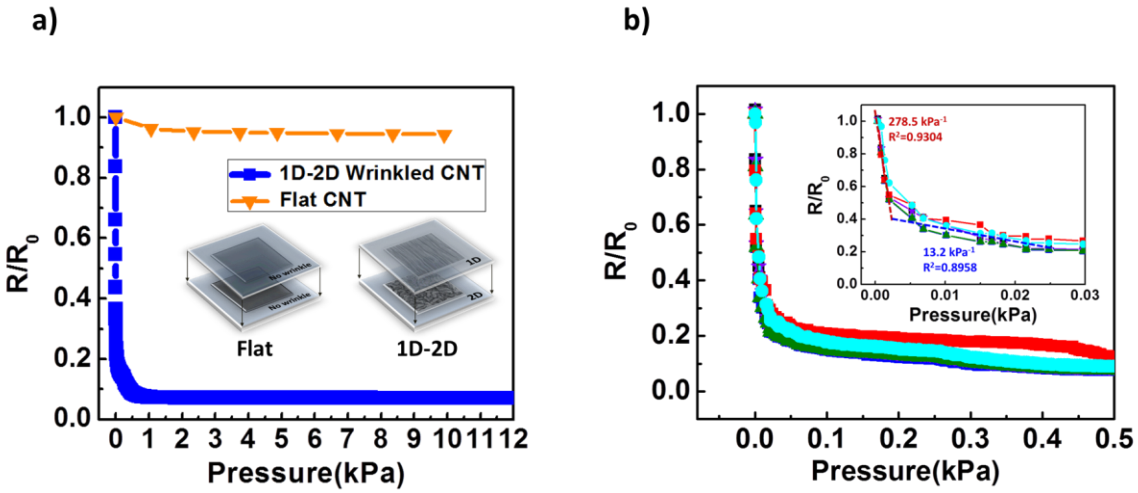

Figure 6.4. Illustration of CNT thin film pressure sensor. a) Piezoresistive response of flat CNT thin film pressure sensor(orange) and Piezoresistive response of 1D-2D wrinkled CNT thin film pressure sensor(blue). b) Six different piezoresistive response of 1D-2D wrinkled CNT thin film pressure sensors (0-0.5 kPa). Inset shows expanded view of the piezoresistive response of 1D-2D wrinkled CNT thin film pressure sensors from 0-30 Pa (each sample denoted with a different color).

The plot in **Figure 6.4** illustrates the piezoresistive response of a 1D-2D wrinkled CNT thin film sensor while applying a normal pressure (R_o~170-190 Ohm). This plot can be separated into two distinct regions from 0-2 Pa and 2-25 Pa. In the first region from 0-2 Pa, the pressure sensitivity was measured to be 278.5 kPa^{-1} showing high linearity of R^2 = 0.9304 as seen in **Figure 6.5**. The piezoresistive response then decreased to approximately 13.2 kPa^{-1} with a linearity of R^2 = 0.8958 (**Figure 6.4b**). At approximately 0.5 kPa, the change in resistance was relatively small. This was due to the wrinkles becoming compressed against each other and not being able to create additional electrical contact points as it was being compressed. The two electrode surfaces after 0.5 kPa were virtually flat against each other as shown by the lower sensitivity in the second region (**Figure 3b**). By incorporating wrinkled structures into the CNT thin film, the pressure sensitivity was improved by at least 12800 times. As seen in **Figure 3b**, the pressure sensitivity was measured to be 278.5 kPa^{-1} while the flat CNT thin film electrodes had a pressure sensitivity of approximately 0.022 kPa^{-1}(**Figure 6.6**).

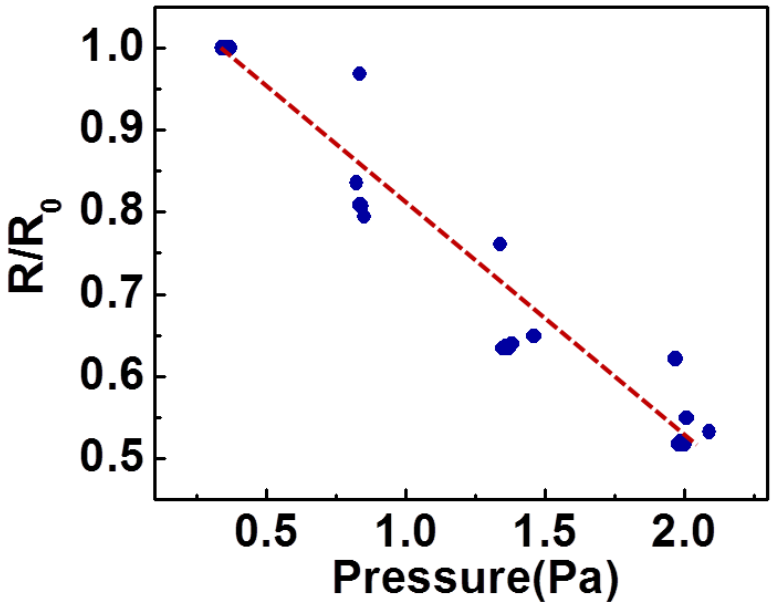

Figure 6.5. Least squares method was used to determine R^2 = .9304 across 6 different samples from 0-2 Pa.

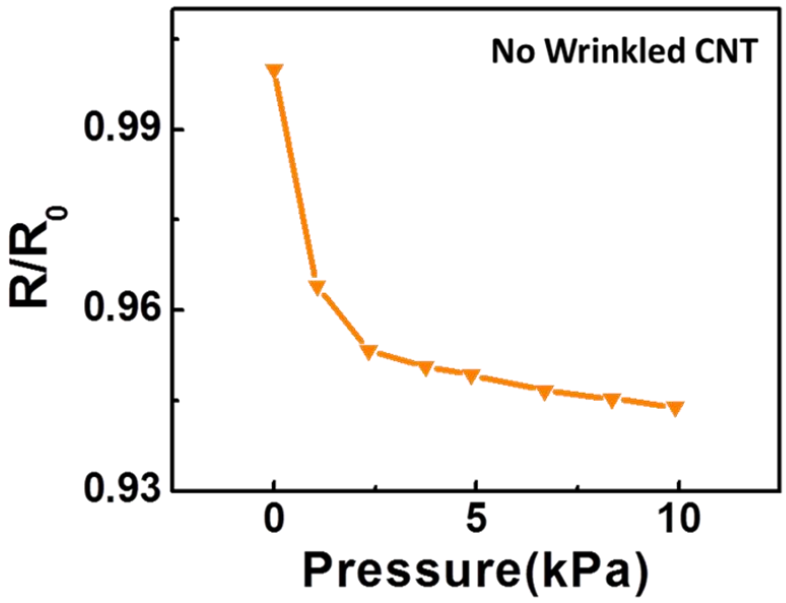

Figure 6.6. Piezoresistive response of flat CNT thin film pressure sensor.

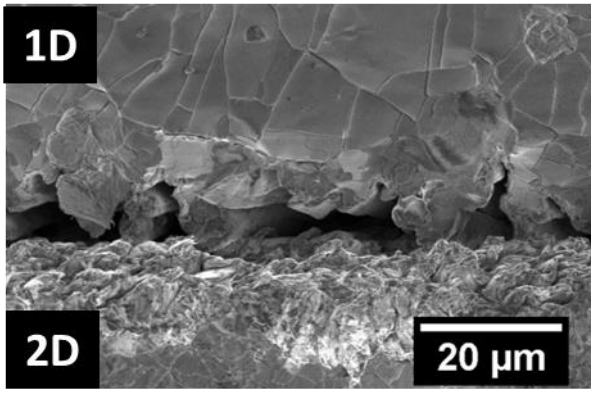

Figure 6.7. Cross sectional SEM image of 2D and 1D wrinkled CNTs compressed against each other.

We previously reported that wrinkled CNT thin films on silicone elastomers can elastically deform in the presence of mechanical strain.[127] We hypothesize that these wrinkled carbon nanotube structures also deform when normal pressures were applied. As these wrinkled structures were compressed, the contacting surface area rapidly increased which resulted in a lowering of electrical resistance between the electrodes. After the structures were compressed against each other, the change in resistance was minimal. The cross section of the wrinkled CNTs compressed against each other can be seen in **Figure 6.2, and 6.7.**

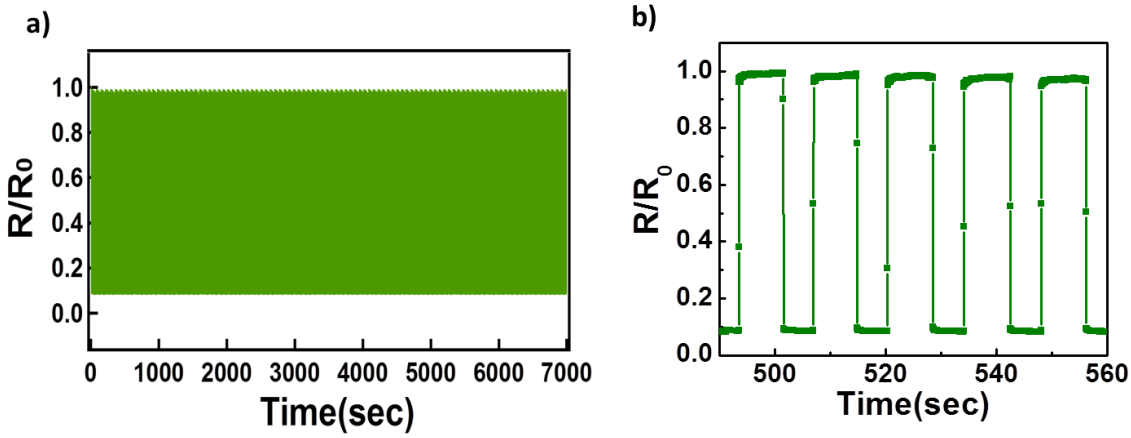

Figure 6.8. a) Piezoresistive response of pressure sensor after 500 cycles of 0.5 kPa applied pressure. b) Inset of 500 cycles displaying piezoresistive response of 5 cyclic loads.

The robustness and repeatability of the wrinkled CNT pressure sensor were tested by applying cyclic pressure. This was accomplished by applying and releasing a load of 0.5 kPa normal to the wrinkled CNT pressure sensor. The piezoresistive response in Figure 4 shows that applying a pressure of 0.5 kPa produces a change of 0.99 which corresponds well with **Figure 6.4b**. As seen in **Figure 6.8** the change in electrical resistance in response to pressure was highly repeatable and stable over the 500 cycles tested displaying a deviation of 0.012 (**Figure 6.9**). The fidelity of the wrinkled structures before and after applying 500 cycles of 0.5kPa was maintained as shown in **Figure 6.10**

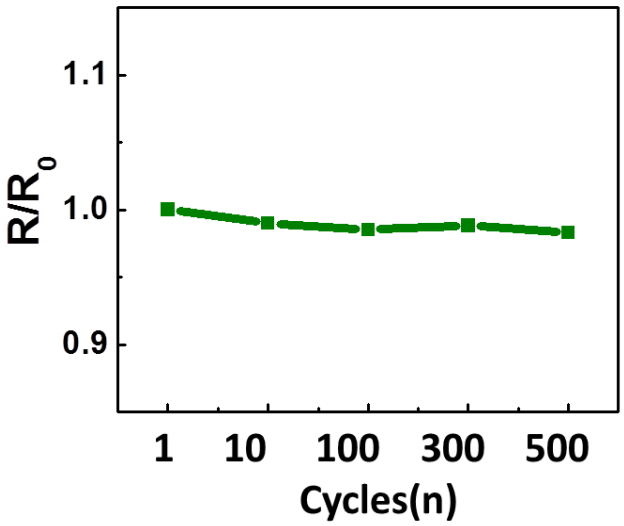

Figure 6.9. Relative change in resistance after a number of cycles with an applied pressure of 0.5 kPa.

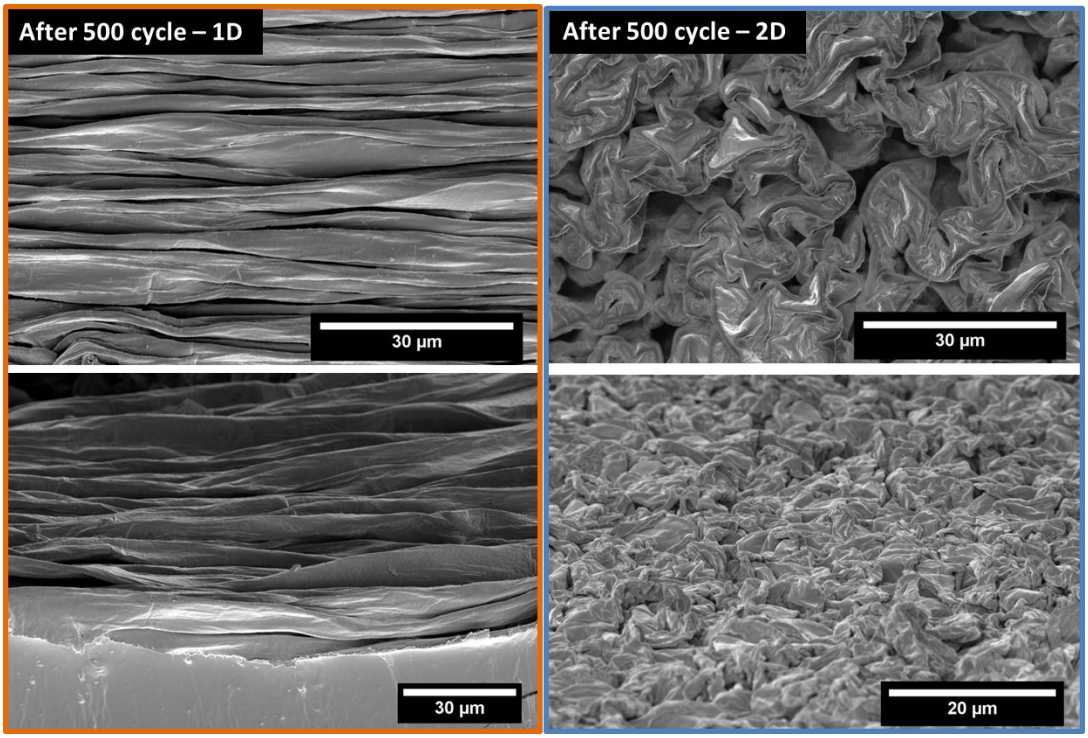

Figure 6.10. Scanning electron microscope images of top down(top) and cross section(down) of 1D and 2D wrinkled topography after 500 cycles.

6.3.3 Human Physiological Signal : Pulsatile blood flow, Voice

To demonstrate wearable applications, detection of pulsatile blood flow and the human voice were pursued. The pressure sensor was mounted on top of the wrist located above the radial artery. The resistive response was then recorded over several pulsatile blood flow cycles. The plot can be seen in **Figure 6.11**. Due to the high response time (<20ms), the pressure sensor was able to distinguish the unique waveform, including the systolic and diastolic peaks, present in arterial pulsatile blood flow. Using the first systolic (SYS1), second systolic (SYS2), and the

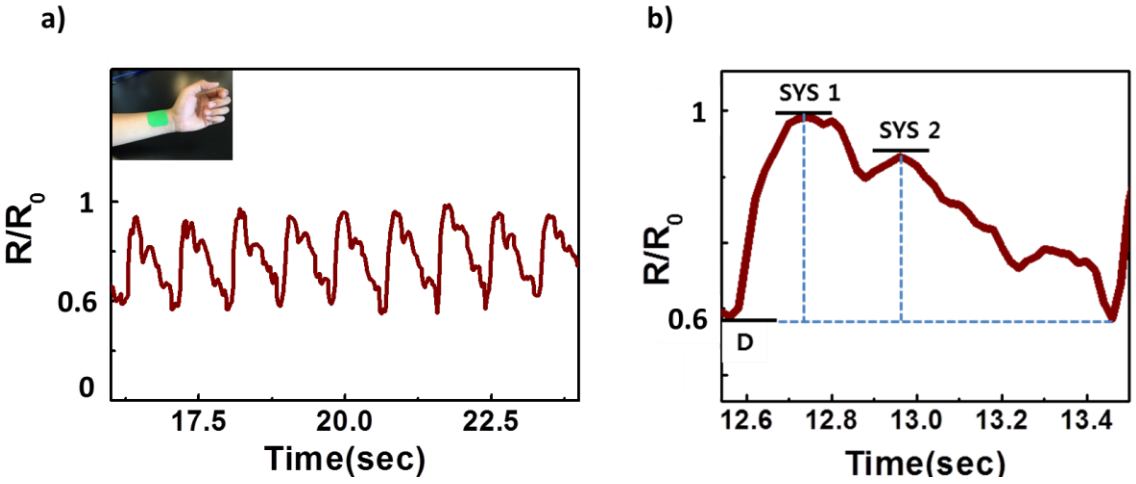

Figure 6.11. a) Pressure sensor was placed on the radial artery of the wrist demonstrating pulsatile blood flow detection. b) Inset of one radial artery pulse waveform with systolic and diastolic pressures indicated.

---

diastolic peak (D), it is possible to calculate the augmentation index (AI) where AI = (SYS2-D)/(SYS1-D).[8,130,131] The augmentation index is a parameter that has been used to assess vascular aging within a patient and has also been related with cardiovascular disease such as atherosclerosis.[130,132,133] The average AI was calculated to be 69.3 ± 6.2% suggesting that the

volunteer was within normal vascular aging.[108,117,130,131] The age of the volunteer with our pressure sensor was 36. The normal range for a person of this age is approximately between 50-75 as seen in **Figure 6.4** of reference. [117]

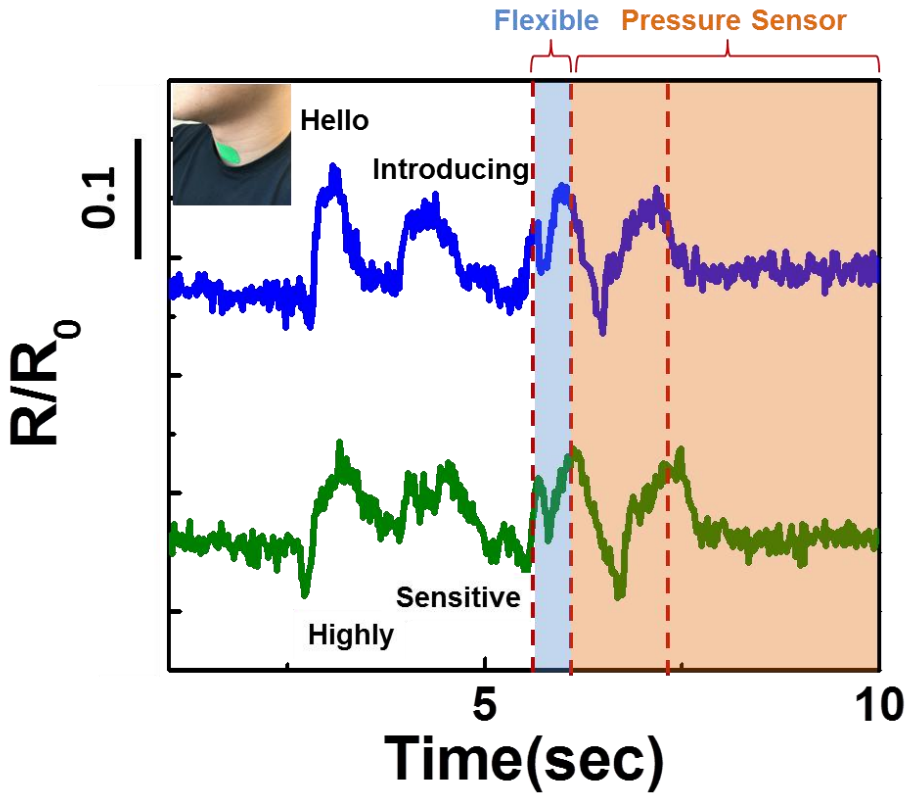

Figure 6.12. After placing the pressure sensor on a volunteer's neck, various phrases were spoken demonstrating unique detection of words. "Hello, Introducing flexible pressure sensor"(blue) and "Highly sensitive flexible pressure sensor"(Green)

For voice detection applications, the pressure sensor was mounted directly over the throat. The electrical response of the pressure sensor was measured while speaking different phrases. As seen in **Figure 6.12**, certain words and phrases can be easily distinguished. As seen in the plot, the words ‘flexible‘ and ‘pressure sensor‘ had similar signal responses when two different phrases were spoken. This shows that these pressure sensors can be used for not just health monitoring applications, but as well as voice detection possibly for communication/translation applications.

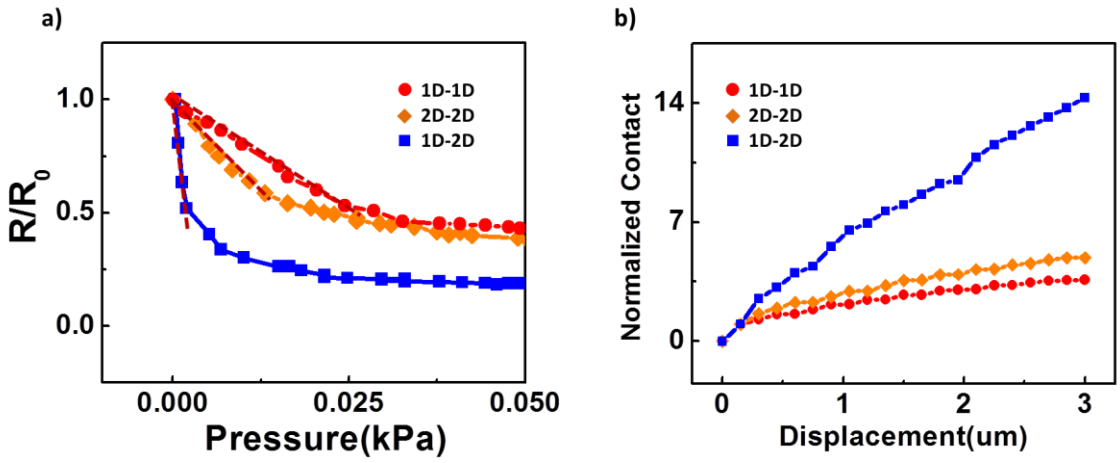

Figure 6.13. a) Piezoresistive response plot and b) Finite elemental analysis of three different combinations of 1D and 2D wrinkled CNT thin films.

6.3.4 Different Wrinkle Combinations

Several different combinations of wrinkle morphologies were tested. As previously reported, PS can shrink biaxially or uniaxially thereby creating different wrinkled morphologies

in functional materials. **Figure 6.2(c,e)** illustrates one dimensional (1D) and two dimensional (2D) wrinkled CNT thin film transferred onto a silicone elastomer. The highest pressure sensitivity was found by combining 1D and 2D wrinkled CNT thin films (**Figure 6.13a**). Due to the high morphology mismatch, the initial surface area contact was low and increased as pressure was applied resulting in a higher pressure sensitivity. A simplified FEA of the 2D-1D contact shows that only some of the wrinkle features are initially in contact, and as the wrinkles deform under pressure, newer contacts are initiated and propagated (**Figure 6.13b, and 6.14**). In comparison, 2D-2D and 1D-1D both had lower pressure sensitivities (26.15 kPa^{-1} and 16.73 kPa^{-1} repectively) than 2D-1D suggesting the geometrical mismatch can lead to higher sensitivities. This strategy can be implemented into similar piezoresistive pressure sensors allowing for detections of subtle pressures.

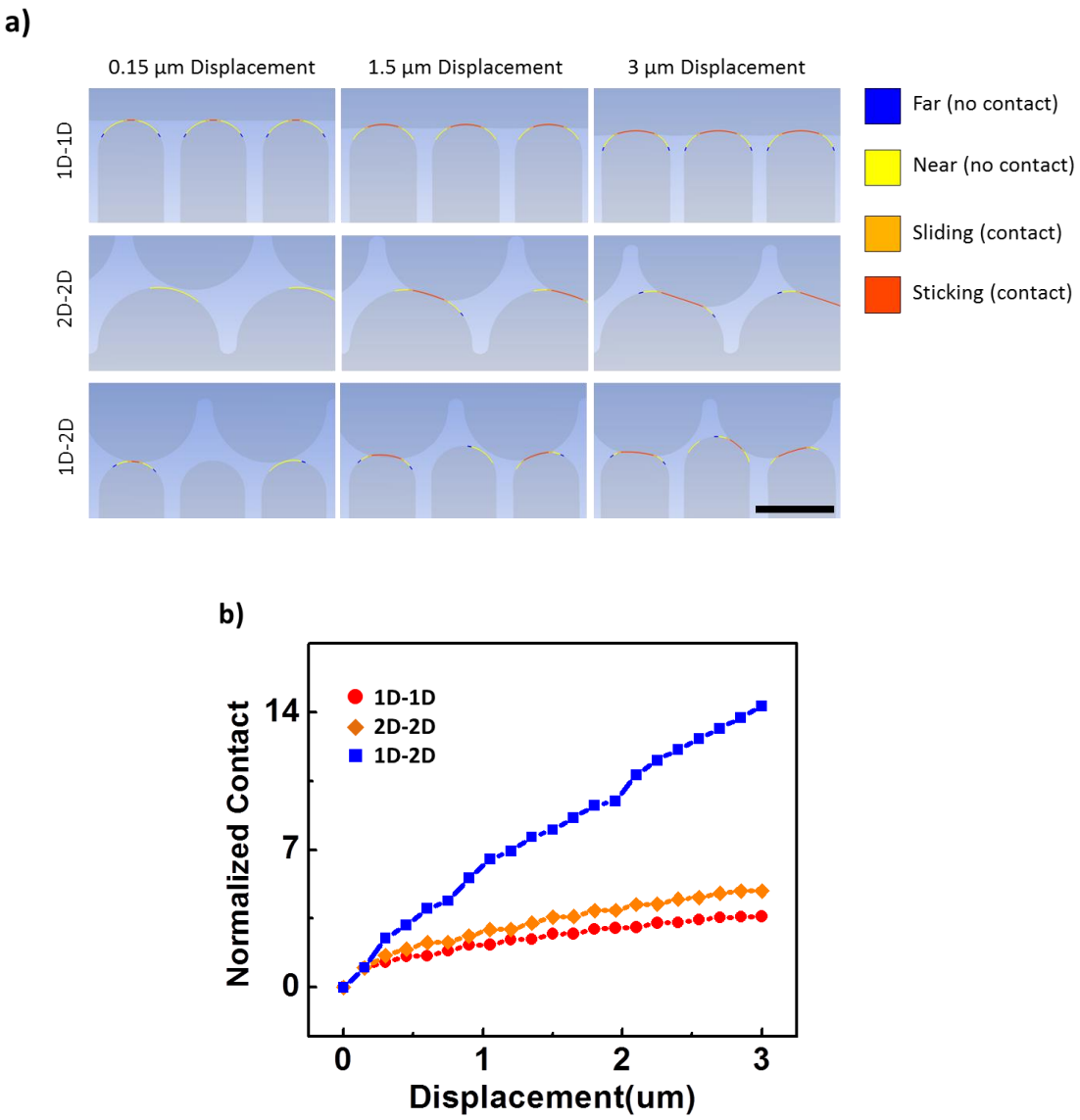

Figure 6.14. (a) Shows a magnified view of the contact for the 1D-1D, 2D-2D, and 1D-2D contact for different displacements. Scale bar is 5 µm. (b) A plot of the normalized nodal contact between the two surfaces, where the initial number of nodes in contact is equal to 1.

6.4. Conclusion

In conclusion, shape memory polymer PS was used to fabricate highly wrinkled CNT thin films using a thermally induced shrinking process. Piezoresistive pressure sensors were then

fabricated by sandwiching two wrinkled CNT thin film electrodes. The highly wrinkled surface allowed for modulation of the contacting surface area when pressures were applied consequently reducing the resistance between the electrodes. Supported by FEA, 1D and 2D wrinkled CNT thin films produced the highest pressure sensitivity due to the high surface roughness mismatch. Radial artery pulsatile blood flow and voice detection applications were then demonstrated by mounting above the wrist and throat respectively. Wrinkle morphology can be finely tuned by shrinking different thicknesses of functional materials as shown by Gabardo et al.[128] Further studies include investigating how different wrinkle morphologies will affect the performance of these piezoresistive pressure sensors. This was the first demonstration of piezoresistive pressure sensors using a rapid prototyping and cost-effective shrinking fabrication process.

CHAPTER 7 : Flexible Capacitance Pressure Sensor for Continuous Blood Flow Monitoring

7.1 Introduction

Wearable electronics have received considerable attention due to a wide variety of applications including continuous monitoring of human physiological signals. [84,134–137] such as respiration[138–140], the heart's electrical activity (electrocardiogram)[114,141–143], sweat biomarkers[144–148], and pulsatile blood flow[8,114,122,149–151]. These applications have been enabled by the fabrication of stretchable and flexible functional materials that can withstand mechanical deformations allowing conformity to the human body. More importantly, wearable electronics have become highly sensitive to physiological signals allowing for detections of weak signals such as pulsatile blood flow.

Within the class of wearable electronics, flexible pressure sensors have been developed to transduce subtle pressures to electrical signals.[110,122,149,152–154] Flexible pressure sensors are often classified by their transduction mechanisms by which they operate including piezoresistive[46,116–118,149,154], piezoelectric[108,110,151,155–157], and piezocapacitance. [22,113,121,152,158–161].

This includes continuous measurements of pulsatile blood flow from the radial artery located on the wrist with flexible pressure sensors. However, the pressure exerted through the epidermis by the radial artery on the wrist is subtle with pressures around 5kPa. The pulsatile blood flow also has a unique waveform that contains information regarding a person's

cardiovascular health.[162] In order to detect this waveform accurately, highly sensitive pressure sensors are desired to detect the small deflections in the radial artery.

The pulsatile blood flow also has a unique waveform that contains information regarding a person's cardiovascular health.[163] In order to detect this waveform accurately, highly sensitive pressure sensors are desired to detect the small deflections in the radial artery.

Pulsatile blood flow propagates throughout the body and can be captured at specific regions of the body. For example, pulsatile blood flow can be detected on the radial artery of a person's wrist. Research has shown that, pulsatile blood flow contains information about cardiovascular health and can be used to calculate blood pressure. Therefore, there are opportunities to be able to continuously monitor a person's blood pressure which may be impactful for a number clinical settings[164]. One such way to measure pulsatile blood flow are pressure sensors.

To date, there has been a considerable focus in developing highly sensitive pressure sensors that are mechanically robust and flexible. These sensors can be classified into three categories: piezoresistive, piezoelectric, and capacitive. Piezoresistive pressure sensors have been characterized with high pressure sensitivities and simple design layouts. [46,116–118,149,154] However, sensitivities rely on surface area which limit the practical sizes of sensors. Piezoelectric sensors have shown high response times but are limited to detecting dynamic responses which limits applications where static pressure is necessary. [108,110,151,155–157]

Capacitive pressure sensors have shown to produce high response times, linear responses, and also have simple design layouts. Typically, capacitive pressure sensors are comprised of two

parallel electrodes with an elastomeric dielectric layer producing a capacitance illustrated by the following equation (2):

$$C = \frac{\varepsilon A}{d} \tag{7.1}$$

C is a capacitance, ε s dielectric constant, A is active surface area, d is distance between two electrode(dielectric distance). As pressure is applied, the elastomeric dielectric layer becomes compressed leading to an increase in capacitance. In comparison to piezoresistive and piezoelectric sensors, capacitive pressures are characterized with low pressure sensitivities due to the small deformation of the dielectric layer. Therefore, there is a need to improve the pressure sensitivities of capacitive pressure sensors to leverage the characteristics of capacitive pressure sensors in human physiological signal detection.

To improve pressure sensitivities, microstructured dielectric layers have been implemented. For example, Mannsfeld et al. molded micropyramidal structures into PDMS dielectric layers which improved pressure sensitivities by five times in pressure regions <2kPa.[153] However, there has yet to be a method that uses a simple fabrication process while also producing robust capacitive pressure sensors with high sensitivities.

In this chapter, a shrinking fabrication process to produce highly wrinkled structures in thin films will be used to fabricate capacitive pressure sensors. In previous studies, we have demonstrated that thermoplastics (e.g polystyrene) can be used to create highly wrinkled micro/nanoscaled structures in thin films. These wrinkle structures provided strain relief allowing brittle thin materials to withstand strains of up to 200%. In addition, we describe that

these structures will also enhance pressure sensitivity allowing for detections of subtle signals such as pulsatile blood flow. In addition, we introduce preliminary experiments allowing to calculate a person's blood pressure from the measured pulsatile blood flow information.

7.2 Experimental Design

7.2.1. Fabrication of capacitance pressure sensor

Gold was patterned by depositing over a shadow mask onto a polystyrene sheet. After removal of the shadow mask, the gold was treated with mercapto(trimethoxy)silane. Polydimethylsiloxane(PDMS) was then spin coated over the gold which chemically reacted with the MPTMS allowing for stronger adhesion. The device was then put into a heated acetone bath, followed by a toluene wash to release the gold from the polystyrene and onto the PDMS. An anisotropically conductive tape (sparkfun) was then attached to the gold thin film to form an electrical connection with a ribbon cable. A 50um Ecoflex layer was then spin coated on top of the device. Afterwards, another transferred gold thin film was then sandwiched on top of the Ecoflex layer.

7.2.2. Structure Characterization

Scanning electron microscope (SEM, FEI Magellan 400 XHR) was used to image the wrinkled topography of the gold thin film. Samples were coated with Ir prior to imaging.

7.2.3. Pressure sensor characterization

A universal tensile machine (UTM) was used to apply controlled amounts of pressure applied to the sensor. The relative change in capacitance of the wrinkled Au-PDMS sensor under applied force was measured using a force gauge (Series 5, Mark-10).and an LCR meter (E4980A, Keysight Tech.) using the 4 point probe method at 1V.

7.2.4. Data acquisition

Sensor was placed directly over the radial artery located on the wrist. A soft foam spacer was attached directly over the overlapping electrodes to create a conformal contact between the skin directly above the artery and the sensor. Measurements were taken with a LCR meter (Keysight E4890A) at 100 kHz at approximately 1 V.

7.2.5. ClearSight System

The ClearSight system is a system that can continuously and noninvasively recorded arterial blood pressure using a finger cuff. (Finapres Medical Systems Finometer MIDI hardware and Beatscope software). Noninvasive continuous arterial blood pressure and heart rate were measured beat-to-beat using the ClearSight system on the index finger with a height calibration system. This uses the volume-clamp method to measure finger arterial pressure. Each side of diodes in the finger cuff, measure changes in artery diameter and change the inflation of the cuff with the diameter remains at the set point. The cuff is inflated or deflated via an air bladder

connected to an air pump.[164] The volume-clamp keeps the diameter of the artery under an inflated finger cuff at a set point, and determines with time changes by arterial pressure

The ClearSight finger cuff with Beatscope software,using a mathematical model, generates an aortic pulse waveform from the finger arterial pressure wave. This computational model accounts the changes in the pulse pressure and waveform shape as the pressure pulse is transmitted down the brachial arteries to the finger arteries. A fluid-filled tube attached between the top of the finger cuff and the subject's heart includes the positioning of the cuff relative to the heart in the computation[165]

7.3 Result and Discussion

7.3.1. Measure sensitivity of Au Capacitance Pressure Sensor

Sensing the pressure is conducted by detecting the change in the capacitance due to the change in the distance between the top and bottom Au wrinkled electrode. Plot of relative change in capacitance($\Delta C/C_0$) as a function of applied pressure, using wrinkled Au/PDMS sensor with and without air bubble(gap) which is incorporated during the fabrication process. Without air bubble on the dielectric layer will slightly increase the capacitance due to decreasing the distance between the top and bottom Au wrinkled electrode as the Au/PDMS sensor is compressed. Introducing the air bubble(gap) into the dielectric layer, will have a better sensing ability due to the combined effect of less pressure required to deform the PDMS substrate and air being driven out of the voids, which is changing the dielectric constant as the Au/PDMS sensor is compressed.

When air bubble is completely flat, sensitivity will increase significantly in the low pressure region. The air bubble enables to change the distance of dielectric layer which is between the top and bottom electrodes under relatively low pressures. So, there will be large rate of change in capacitance under small changes in pressure.

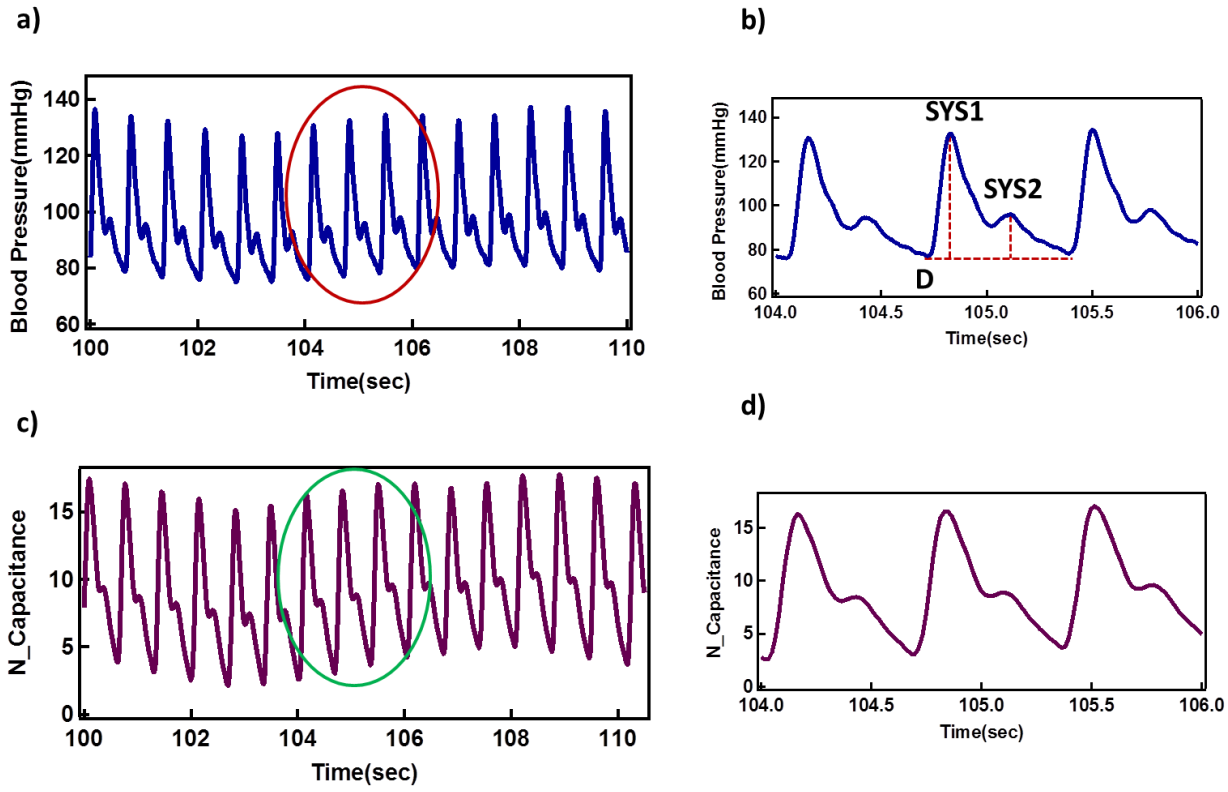

Figure 7.1. (a) Shows blood pulse measurement from ClearSight system. (b) expanded pulsatile peaks of ClearSight system. (c) blood pulse measurement from Au wrinkled pressure sensor. (d) expanded pulsatile flow of Au wrinkled pressure sensor.

Also compare with flat Au electrode and wrinkled Au electrode. Flat Au electrode will have high relaxation time after compression due to irreversibility and lack of deformable of flat Au electrode surface. Wrinkled Au electrode with PDMS film provides to elastically deform the

substrate by external pressure, therefore stores and releases the energy reversibility and minimizing the relaxation time related problems.

7.3.2. Correlating ClearSight with wrinkled Au capacitance sensor

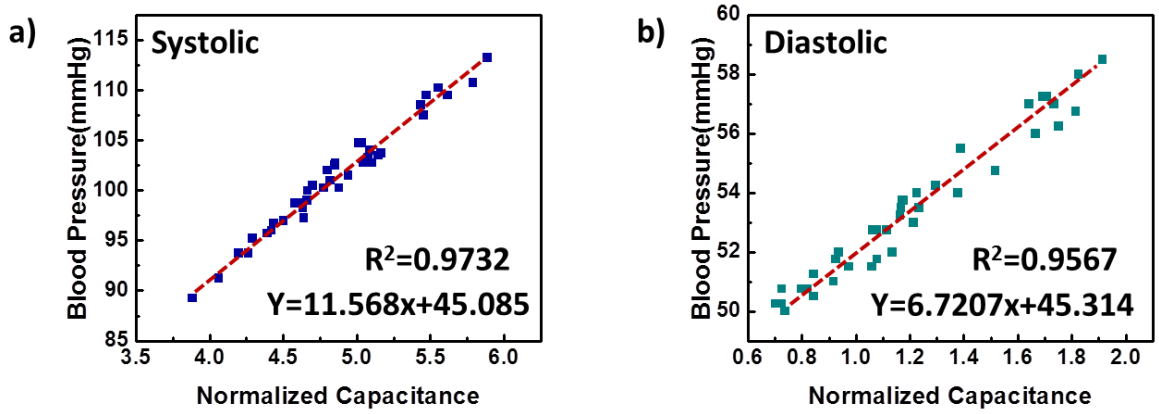

Figure 7.2. After syncing the time series data from the ClearSight system and the pressure sensor, correlated the normalized change in capacitance with blood pressure, (a) systolic and (b) diastolic.

Currently, we are focused on correlating pulsatile blood flow, measured using flexible capacitive pressure sensors, with blood pressure to show clinical relevance in wearable health technology. This is accomplished by simultaneously measuring the force exerted from the radial artery using a capacitive pressure sensor and the blood pressure using a ClearSight system. The ClearSight system (Edwards Lifesciences) is an FDA approved continuous hemodynamic monitoring system that uses an inflatable finger cuff to measure blood pressure. The ClearSight system in this study is being used as a proxy for blood pressure to which the pulsatile blood flow measured from the capacitive pressure sensor is being compared to. Correlations are being made

by measuring the blood pressure from the left index finger using the ClearSight system, and measuring the pulsatile blood flow from the radial artery on the right arm using the capacitive pressure sensor at 300kHz and 1V (E4980AL). After syncing the time series data from the ClearSight system and the pressure sensor, we have been correlating the normalized change in capacitance with blood pressure.

REFERENCES

[1] N. Lu, C. Lu, S. Yang, J. Rogers, *Adv. Funct. Mater.* **2012**, *22*, 4044.

[2] S. Luo, T. Liu, *Adv. Mater.* **2013**, *25*, 5650.

[3] F. Axisa, P. M. Schmitt, C. Gehin, G. Delhomme, E. Mcadams, A. Dittmar, A. S. Background, *IEEE Trans. Inf. Technol. Biomed.* **2005**, *9*, 325.

[4] M. Sung, C. Marci, A. Pentland, *J. Neuroeng. Rehabil.* **2005**, *2*, 21.

[5] J. Hwang, J. Jang, K. Hong, K. N. Kim, J. H. Han, K. Shin, C. E. Park, *Carbon N. Y.* **2011**, *49*, 106.

[6] J. Zhang, J. Liu, R. Zhuang, E. Mäder, G. Heinrich, S. Gao, *Adv. Mater.* **2011**, *23*, 3392.

[7] R. C. Webb, A. P. Bonifas, A. Behnaz, Y. Zhang, K. J. Yu, H. Cheng, M. Shi, Z. Bian, Z. Liu, Y.-S. Kim, W.-H. Yeo, J. S. Park, J. Song, Y. Li, Y. Huang, A. M. Gorbach, J. A. Rogers, *Nat. Mater.* **2013**, *12*, 938.

[8] G. Schwartz, B. C.-K. Tee, J. Mei, A. L. Appleton, D. H. Kim, H. Wang, Z. Bao, *Nat. Commun.* **2013**, *4*, 1859.

[9] B. Hu, W. Chen, J. Zhou, *Sensors Actuators, B Chem.* **2013**, *176*, 522.

[10] M. Hempel, D. Nezich, J. Kong, M. Hofmann, *Nano Lett.* **2012**, *12*, 5714.

[11] L. Persano, C. Dagdeviren, Y. Su, Y. Zhang, S. Girardo, D. Pisignano, Y. Huang, J. A. Rogers, *Nat. Commun.* **2013**, *4*, 1633.

[12] H. Vandeparre, D. Watson, S. P. Lacour, *Appl. Phys. Lett.* **2013**, *103*, 2.

[13] Y. Qi, J. Kim, T. D. Nguyen, B. Lisko, P. K. Purohit, M. C. McAlpine, *Nano Lett.* **2011**, *11*, 1331.

[14] D.-Y. Khang, H. Jiang, Y. Huang, J. A. Rogers, *Science (80-.).* **2006**, *311*, 208.

[15] S. P. Lacour, D. Chan, S. Wagner, T. Li, Z. Suo, *Appl. Phys. Lett.* **2006**, *88*, 1.

[16] M. Zheng, W. Li, M. Xu, N. Xu, P. Chen, M. Han, B. Xie, *Nanoscale* **2014**, *6*, 3930.

[17] H. Wang, X. Han, X. Ou, C.-S. Lee, X. Zhang, S.-T. Lee, *Nanoscale* **2013**, *5*, 8172.

[18] K. Takei, T. Takahashi, J. C. Ho, H. Ko, A. G. Gillies, P. W. Leu, R. S. Fearing, A. Javey, *Nat. Mater.* **2010**, *9*, 821.

[19] X. Xiao, L. Yuan, J. Zhong, T. Ding, Y. Liu, Z. Cai, Y. Rong, H. Han, J. Zhou, Z. L. Wang, *Adv. Mater.* **2011**, *23*, 5440.

[20] A. B. Dalton, S. Collins, E. Muñoz, J. M. Razal, V. H. Ebron, J. P. Ferraris, J. N. Coleman, B. G. Kim, R. H. Baughman, *Nature* **2003**, *423*, 703.

[21] Q. Fan, Z. Qin, S. Gao, Y. Wu, J. Pionteck, E. Mäder, M. Zhu, *Carbon N. Y.* **2012**, *50*, 4085.

[22] D. J. Lipomi, M. Vosgueritchian, B. C.-K. Tee, S. L. Hellstrom, J. a. Lee, C. H. Fox, Z. Bao, *Nat. Nanotechnol.* **2011**, *6*, 788.

[23] F. Mirri, A. W. K. Ma, T. T. Hsu, N. Behabtu, S. L. Eichmann, C. C. Young, D. E. Tsentalovich, M. Pasquali, *ACS Nano* **2012**, *6*, 9737.

[24] Y. Shang, X. He, Y. Li, L. Zhang, Z. Li, C. Ji, E. Shi, P. Li, K. Zhu, Q. Peng, C. Wang, X. Zhang, R. Wang, J. Wei, K. Wang, H. Zhu, D. Wu, A. Cao, *Adv. Mater.* **2012**, *24*, 2896.

[25] T. Yamada, Y. Hayamizu, Y. Yamamoto, Y. Yomogida, A. Izadi-Najafabadi, D. N. Futaba, K. Hata, *Nat. Nanotechnol.* **2011**, *6*, 296.

[26] S. Tadakaluru, W. Thongsuwan, P. Singjai, *Sensors* **2014**, *14*, 868.

[27] S. H. Bae, Y. Lee, B. K. Sharma, H. J. Lee, J. H. Kim, J. H. Ahn, *Carbon N. Y.* **2013**, *51*, 236.

[28] H. Tian, Y. Shu, Y. Cui, W. Mi, Y. Yang, T. Ren, *Nanoscale* **2014**, 699.

[29] H. Tian, Y. Shu, Y.-L. Cui, W.-T. Mi, Y. Yang, D. Xie, T.-L. Ren, *Nanoscale* **2014**, *6*, 699.

[30] Y. Wang, L. Wang, T. Yang, X. Li, X. Zang, M. Zhu, K. Wang, D. Wu, H. Zhu, *Adv. Funct. Mater.* **2014**, *24*, 4666.

[31] K. S. Kim, Y. Zhao, H. Jang, S. Y. Lee, J. M. Kim, K. S. Kim, J.-H. Ahn, P. Kim, J.-Y. Choi, B. H. Hong, *Nature* **2009**, *457*, 706.

[32] D. Kang, P. V. Pikhitsa, Y. W. Choi, C. Lee, S. S. Shin, L. Piao, B. Park, K.-Y. Suh, T. Kim, M. Choi, *Nature* **2014**, *516*, 222.

[33] X. Li, R. Zhang, W. Yu, K. Wang, J. Wei, D. Wu, A. Cao, Z. Li, Y. Cheng, Q. Zheng, R. S. Ruoff, H. Zhu, *Sci. Rep.* **2012**, *2*, DOI 10.1038/srep00870.

[34] C. Yan, J. Wang, W. Kang, M. Cui, X. Wang, C. Y. Foo, K. J. Chee, P. S. Lee, *Adv. Mater.* **2014**, *26*, 2022.

[35] R. H. Baughman, A. A. Zakhidov, W. A. de Heer, *Science (80-.).* **2002**, *297*, 787.

[36] S. J. Tans, M. H. Devoret, H. Dai, A. Thess, R. E. Smalley, L. J. Geerligs, C. Dekker, *Nature* **1997**, *386*, 474.

[37] R. S. Ruoff, D. C. Lorents, *Carbon N. Y.* **1995**, *33*, 925.

[38] M. M. J. Treacy, T. W. Ebbesen, J. M. Gibson, *Nature* **1996**, *381*, 678.

[39] M. H. Andrew Ng, L. T. Hartadi, H. Tan, C. H. Patrick Poa, *Nanotechnology* **2008**, *19*, 205703.

[40] J. M. Harris, G. R. S. Iyer, A. K. Bernhardt, J. Y. Huh, S. D. Hudson, J. a Fagan, E. K. Hobbie, H. E. T. Al, *ACS Nano* **2011**, 881.

[41] S. Ryu, P. Lee, J. B. Chou, R. Xu, R. Zhao, A. J. Hart, S. Kim, *ACS Nano* **2015**, *9*, 5929.

[42] M. L. Hammock, A. Chortos, B. C. K. Tee, J. B. H. Tok, Z. Bao, *Adv. Mater.* **2013**, *25*, 5997.

[43] J. Kim, M. Lee, H. J. Shim, R. Ghaffari, H. R. Cho, D. Son, Y. H. Jung, M. Soh, C. Choi, S. Jung, K. Chu, D. Jeon, S.-T. Lee, J. H. Kim, S. H. Choi, T. Hyeon, D.-H. Kim, *Nat. Commun.* **2014**, *5*, 5747.

[44] V. Maheshwari, *Science (80-.).* **2006**, *312*, 1501.

[45] Z. L. W. Wenzhuo Wu,Xiaonan Wen, *Science (80-.).* **2013**, *340*, DOI 10.1126/science.1234855.

[46] C. Pang, G.-Y. Lee, T. Kim, S. M. Kim, H. N. Kim, S.-H. Ahn, K.-Y. Suh, *Nat. Mater.* **2012**, *11*, 795.

[47] J. Ge, L. Sun, F. R. Zhang, Y. Zhang, L. A. Shi, H. Y. Zhao, H. W. Zhu, H. L. Jiang, S. H. Yu, *Adv. Mater.* **2015**, 722.

[48] J. D. Pegan, A. Y. Ho, M. Bachman, M. Khine, *Lab Chip* **2013**, *13*, 4205.

[49] S. Lin, E. K. Lee, N. Nguyen, M. Khine, *Lab Chip* **2014**, *14*, 3475.

[50] K. Lu, M. Accorsi, J. Leonard, **2001**, 1017.

[51] Z. Y. Huang, W. Hong, Z. Ã. Suo, **2005**, *53*, 2101.

[52] Bowden,Ned, S. Brittain, A. G. Evans, Hutchinson, J. W, G. M. Whitesides, **1998**, *393*, 146.

[53] D. G. Roddeman, J. Drukker, C. W. J. Oomens, J. D. Janssen, **2017**, *54*.

[54] M. Ortiz, G. G. I. Ia, **1994**, *42*.

[55] N. Bowden, W. T. S. Huck, K. E. Paul, G. M. Whitesides, N. Bowden, W. T. S. Huck, K. E. Paul, G. M. Whitesides, **2007**, *2557*, 1.

[56] E. Sharon, B. Roman, M. Marder, G. Shin, **2002**, *419*.

[57] J. Genzer, J. Groenewold, **2006**, DOI 10.1039/b516741h.

[58] E. P. Chan, A. J. Crosby, **2006**, 324.

[59] B. E. P. Chan, E. J. Smith, R. C. Hayward, A. J. Crosby, **2008**, 711.

[60] S. P. Lacour, S. Wagner, Z. Huang, Z. Suo, **2013**, *2404*, DOI 10.1063/1.1565683.

[61] A. Schweikart, A. Horn, A. Boker, A. Fery, *Controlled Wrinkling as a Novel Method for the Fabrication of Patterned Surfaces*, Advanced Polymer Science, **2010**.

[62] J. Fukuda, T. Ohzono, *Nat. Commun.* **2012**, *3*, 701.

[63] B. D. P. Holmes, A. J. Crosby, **2007**, 3589.

[64] H. E. Jeong, M. K. Kwak, K. Y. Suh, **2010**, *26*, 2223.

[65] C. M. Stafford, C. Harrison, K. L. Beers, A. Karim, E. J. Amis, M. R. Vanlandingham, H. Kim, W. Volksen, R. D. Miller, E. V. A. E. Simonyi, **2004**, *3*, 2004.

[66] T. Ohzono, M. Shimomura, **2004**, 1.

[67] M. Watanabe, **2005**, 1532.

[68] A. Materials, **2017**, *4095*, DOI 10.1002/1521-4095(20021002)14.

[69] A. Lendlein, S. Kelch, **n.d.**

[70] C. J. Vorosmarty, A. J. Kettner, P. Green, B. J. Mcelroy, J. C. Van Uchelen, **2008**, 720.

[71] A. J. Harvey, Y. N. Parkhomenko, E. A. Skryleva, U. Bangert, A. Gutie, **2009**, *7*, 3.

[72] A. V Eletskii, **n.d.**, DOI 10.1070/PU2004v047n11ABEH002017.

[73] K. F. Akhmadishina, I. I. Bobrinetskii, I. A. Komarov, A. M. Malovichko, V. K. Nevolin, V. A. Petukhov, A. V Golovin, A. O. Zalevskii, **2013**, *8*, 721.

[74] W. Zhang, W. Zhang, **2009**, *2009*, DOI 10.1155/2009/160698.

[75] N. Lett., *Hu, L. Heclht, D.S. Gruner, G* **2004**, *4*, 2513.

[76] K. Bradley, J. C. P. Gabriel, G. Grüner, *Nano Lett.* **2003**, *3*, 1353.

[77] R. C. Tenent, T. M. Barnes, J. D. Bergeson, A. J. Ferguson, B. To, L. M. Gedvilas, M. J. Heben, J. L. Blackburn, *Adv. Mater.* **2009**, *21*, 3210.

[78] C. Preston, D. Song, J. Dai, Z. Tsinas, J. Bavier, J. Cumings, V. Ballarotto, L. Hu, *Nano Res.* **2015**, *8*, 2242.

[79] J. Lu, M. Lu, A. Bermak, S. Member, Y. Lee, *Proceeding 7th IEEE Int. Conf. Nanotechnol.* **2007**, 1240.

[80] M. Amjadi, Y. J. Yoon, I. Park, *Nanotechnology* **2015**, *26*, 375501.

[81] J. Park, Y. Lee, J. Hong, M. Ha, Y. Do Jung, H. Lim, S. Y. Kim, H. Ko, *ACS Nano* **2014**, *8*, 4689.

[82] X. Wang, Y. Gu, Z. Xiong, Z. Cui, **2013**, DOI 10.1002/adma.

[83] S. Gong, W. Schwalb, Y. Wang, Y. Chen, Y. Tang, J. Si, B. Shirinzadeh, W. Cheng, *Nat. Commun.* **2014**, *5*, 1.

[84] D.-H. Kim, N. Lu, R. Ma, Y.-S. Kim, R.-H. Kim, S. Wang, J. Wu, S. M. Won, H. Tao, A. Islam, K. J. Yu, T. Kim, R. Chowdhury, M. Ying, L. Xu, M. Li, H.-J. Chung, H. Keum, M. McCormick, P. Liu, Y. Zhang, F. G. Omenetto, Y. Huang, T. Coleman, J. A. Rogers, *Science (80-.).* **2011**, *333*, 838.

[85] X. Liu, Y. Zhu, M. W. Nomani, X. Wen, T.-Y. Hsia, G. Koley, *J. Micromechanics Microengineering* **2013**, *23*, 025022.

[86] F. Xu, Y. Zhu, *Adv. Mater.* **2012**, *24*, 5117.

[87] X. Chen, J. Shao, N. An, X. Li, H. Tian, C. Xu, Y. Ding, *J. Mater. Chem. C* **2015**, *3*, 11806.

[88] A. V Zaretski, S. E. Root, A. Savchenko, E. Molokanova, A. D. Printz, L. Jibril, G. Arya, M. Mercola, D. J. Lipomi, **2016**, DOI 10.1021/acs.nanolett.5b04821.

[89] D. J. Lipomi, M. Vosgueritchian, B. C.-K. Tee, S. L. Hellstrom, J. a Lee, C. H. Fox, Z. Bao, *Nat. Nanotechnol.* **2011**, *6*, 788.

[90] J. K. Paik, R. K. Kramer, R. J. Wood, *IEEE Int. Conf. Intell. Robot. Syst.* **2011**, 414.

[91] G. T. Pham, Y. Bin Park, Z. Liang, C. Zhang, B. Wang, *Compos. Part B Eng.* **2008**, *39*, 209.

[92] S. Lin, E. K. Lee, M. Khine, *Lab Chip* **2014**, 3475.

[93] Y. Huang, Y. Wang, L. Xiao, H. Liu, W. Dong, Z. Yin, *Lab Chip* **2014**, *14*, 4205.

[94] C. C. Fu, A. Grimes, M. Long, C. G. L. Ferri, B. D. Rich, S. Ghosh, S. Ghosh, L. P. Lee, A. Gopinathan, M. Khine, *Adv. Mater.* **2009**, *21*, 4472.

[95] J. Kim, S.-J. Park, T. Nguyen, M. Chu, J. D. Pegan, M. Khine, *Appl. Phys. Lett.* **2016**, *108*, 061901.

[96] C. F. Guo, T. Sun, Q. Liu, Z. Suo, Z. Ren, *Nat. Commun.* **2014**, *5*, 1.

[97] S. Michelle, **2013**, DOI 10.1039/c3lc50588j.

[98] J. O'Neill, J. Lu, R. Dockter, T. Kowalewski, in *Proc. - IEEE Int. Conf. Robot. Autom.*, **2015**, pp. 624–629.

[99] M. O. Culjat, C.-H. King, M. L. Franco, C. E. Lewis, J. W. Bisley, E. P. Dutson, W. S. Grundfest, *Conf. Proc. IEEE Eng. Med. Biol. Soc.* **2008**, *2008*, 1930.

[100] X. Zhao, Q. Hua, R. Yu, Y. Zhang, C. Pan, *Adv. Electron. Mater.* **2015**, *1*, 1.

[101] A. N. Sokolov, B. C.-K. Tee, C. J. Bettinger, J. B.-H. Tok, Z. Bao, *Acc. Chem. Res.* **2012**, *45*, 361.

[102] M. J. Cima, *Nat. Biotechnol.* **2014**, *32*, 642.

[103] M. Kaltenbrunner, T. Sekitani, J. Reeder, T. Yokota, K. Kuribara, T. Tokuhara, M. Drack, R. Schwödiauer, I. Graz, S. Bauer-Gogonea, S. Bauer, T. Someya, *Nature* **2013**, *499*, 458.

[104] W. Honda, S. Harada, T. Arie, S. Akita, K. Takei, *Adv. Funct. Mater.* **2014**, *24*, 3299.

[105] L. Cai, L. Song, P. Luan, Q. Zhang, N. Zhang, Q. Gao, D. Zhao, X. Zhang, M. Tu, F. Yang, W. Zhou, Q. Fan, J. Luo, W. Zhou, P. M. Ajayan, S. Xie, *Sci. Rep.* **2013**, *3*, 1.

[106] J. a Rogers, T. Someya, Y. Huang, *Science* **2010**, *327*, 1603.

[107] P. Gutruf, S. Walia, M. Nur Ali, S. Sriram, M. Bhaskaran, *Appl. Phys. Lett.* **2014**, *104*, 021908.

[108] C. Dagdeviren, Y. Su, P. Joe, R. Yona, Y. Liu, Y.-S. Kim, Y. Y. Huang, A. R. Damadoran, J. Xia, L. W. Martin, J. a Rogers, *Nat. Commun.* **2014**, *5*, 4496.

[109] J. Dzuba, G. Vanko, M. Držk, I. Rýger, V. Kutiš, J. Zehetner, T. Lalinský, *Appl. Phys. Lett.* **2015**, *107*, DOI 10.1063/1.4931436.

[110] J. H. Lee, H. J. Yoon, T. Y. Kim, M. K. Gupta, J. H. Lee, W. Seung, H. Ryu, S. W. Kim, *Adv. Funct. Mater.* **2015**, *25*, 3203.

[111] Y.-M. Chen, S.-M. He, C.-H. Huang, C.-C. Huang, W.-P. Shih, C.-L. Chu, J. Kong, J. Li, C.-Y. Su, *Nanoscale* **2016**, *8*, 3555.

[112] K. F. Lei, K.-F. Lee, M.-Y. Lee, *Microelectron. Eng.* **2012**, *99*, 1.

[113] J. Wang, J. Jiu, M. Nogi, T. Sugahara, S. Nagao, H. Koga, P. He, K. Suganuma, *Nanoscale* **2015**, *7*, 2926.

[114] N. Luo, W. Dai, C. Li, Z. Zhou, L. Lu, C. C. Y. Poon, S. C. Chen, Y. Zhang, N. Zhao, *Adv. Funct. Mater.* **2016**, *26*, 1178.

[115] Y. Shu, H. Tian, Y. Yang, C. Li, Y. Cui, W. Mi, Y. Li, Z. Wang, N. Deng, B. Peng, T.-L. Ren, *Nanoscale* **2015**, *7*, 8636.

[116] B. Su, S. Gong, Z. Ma, L. W. Yap, W. Cheng, *Small* **2015**, *11*, 1886.

[117] Z. Wang, S. Wang, J. Zeng, X. Ren, A. J. Y. Chee, B. Y. S. Yiu, W. C. Chung, Y. Yang, A. C. H. Yu, R. C. Roberts, A. C. O. Tsang, K. W. Chow, P. K. L. Chan, *Small* **2016**, 3827.

[118] H. Bin Yao, J. Ge, C. F. Wang, X. Wang, W. Hu, Z. J. Zheng, Y. Ni, S. H. Yu, *Adv. Mater.* **2013**, *25*, 6692.

[119] S. E. Zhu, M. Krishna Ghatkesar, C. Zhang, G. C. A. M. Janssen, *Appl. Phys. Lett.* **2013**, *102*, 2014.

[120] K. Il Park, J. H. Son, G. T. Hwang, C. K. Jeong, J. Ryu, M. Koo, I. Choi, S. H. Lee, M. Byun, Z. L. Wang, K. J. Lee, *Adv. Mater.* **2014**, *26*, 2514.

[121] S. Yao, Y. Zhu, *Nanoscale* **2014**, *6*, 2345.

[122] Y. Zang, F. Zhang, D. Huang, X. Gao, C.-A. Di, D. Zhu, *Nat. Commun.* **2015**, *6*, 6269.

[123] J. Park, Y. Lee, J. Hong, M. Ha, Y.-D. Jung, H. Lim, S. Y. Kim, H. Ko, *ACS Nano* **2014**, *8*, 4689.

[124] X. Wang, Y. Gu, Z. Xiong, Z. Cui, T. Zhang, *Adv. Mater.* **2014**, *26*, 1336.

[125] Y. Wei, S. Chen, X. Dong, Y. Lin, L. Liu, *Carbon N. Y.* **2017**, *113*, 395.

[126] T. Q. Trung, N.-E. Lee, *Adv. Mater.* **2016**, n/a.

[127] S. Park, J. Kim, M. Chu, M. Khine, **2016**, DOI 10.1002/admt.201600053.

[128] C. M. Gabardo, Y. Zhu, L. Soleymani, J. M. Moran-Mirabal, *Adv. Funct. Mater.* **2013**, n/a.

[129] J. M. Nokes, R. Liedert, M. Kim, A. Siddiqui, M. Chu, E. Lee, M. Khine, **2015**, 1.

[130] K. Kohara, Y. Tabara, A. Oshiumi, Y. Miyawaki, T. Kobayashi, T. Miki, *Am. J. Hypertens.* **2005**, *18*, 14.

[131] J. A. Chirinos, J. G. Kips, M. J. Roman, J. Medina-Lezama, Y. Li, A. J. Woodiwiss, G. R. Norton, Yasmin, L. Van Bortel, J. G. Wang, J. R. Cockcroft, R. B. Devereux, I. B. Wilkinson, P. Segers, C. M. McEniery, *Hypertension* **2011**, *57*, 1108.

[132] M. T. Schram, R. M. . Henry, R. A. J. . van Dijk, P. J. Kostense, J. M. Dekker, G. Nijpels, R. J. Heine, L. M. Bouter, N. Westerhof, C. D. A. Stehouwer, *Hypertension* **2004**, *43*.

[133] J. L. Izzo, *Curr. Opin. Cardiol.* **2004**, *19*, 341.

[134] Y. Khan, A. E. Ostfeld, C. M. Lochner, A. Pierre, A. C. Arias, **2016**, 4373.

[135] M. Amjadi, K.-U. Kyung, I. Park, M. Sitti, *Adv. Funct. Mater.* **2016**, *26*, 1678.

[136] S. Patel, H. Park, P. Bonato, L. Chan, M. Rodgers, *J. Neuroeng. Rehabil.* **2012**, *9*, 21.

[137] A. J. Bandodkar, J. Wang, *Trends Biotechnol.* **2014**, *32*, 363.

[138] L. Cai, L. Song, P. Luan, Q. Zhang, N. Zhang, Q. Gao, D. Zhao, X. Zhang, M. Tu, F. Yang, W. Zhou, Q. Fan, J. Luo, W. Zhou, P. M. Ajayan, S. Xie, *Sci. Rep.* **2013**, *3*, 3048.

[139] K. P. Cohen, W. M. Ladd, D. M. Beams, W. S. Sheers, R. G. Radwin, W. J. Tompkins, J. G. Webster, *IEEE Trans. Biomed. Eng.* **1997**, *44*, 555.

[140] M. Amjadi, M. Turan, C. P. Clementson, M. Sitti, **n.d.**, DOI 10.1021/acsami.5b12588.

[141] T. Kim, J. Park, J. Sohn, D. Cho, S. Jeon, *ACS Nano* **2016**, acsnano.6b01355.

[142] S. Xu, Y. Zhang, L. Jia, K. E. Mathewson, K.-I. Jang, J. Kim, H. Fu, X. Huang, P. Chava, R. Wang, S. Bhole, L. Wang, Y. J. Na, Y. Guan, M. Flavin, Z. Han, Y. Huang, J. a Rogers, *Science* **2014**, *344*, 70.

[143] W.-H. Yeo, Y.-S. Kim, J. Lee, A. Ameen, L. Shi, M. Li, S. Wang, R. Ma, S. H. Jin, Z.

Kang, Y. Huang, J. A. Rogers, *Adv. Mater.* **2013**, *25*, 2773.

[144] A. J. Bandodkar, W. Jia, C. Yardımcı, X. Wang, J. Ramirez, J. Wang, *Anal. Chem.* **2015**, *87*, 394.

[145] X. Huang, Y. Liu, K. Chen, W.-J. Shin, C.-J. Lu, G.-W. Kong, D. Patnaik, S.-H. Lee, J. F. Cortes, J. A. Rogers, *Small* **2014**, *10*, 3083.

[146] G. Liu, C. Ho, N. Slappey, Z. Zhou, S. E. E. Snelgrove, M. Brown, A. Grabinski, X. Guo, Y. Chen, K. Miller, J. Edwards, T. Kaya, *Sensors Actuators, B Chem.* **2016**, *227*, 35.

[147] D. P. Rose, M. E. Ratterman, D. K. Griffin, L. Hou, N. Kelley-Loughnane, R. R. Naik, J. A. Hagen, I. Papautsky, J. C. Heikenfeld, *IEEE Trans. Biomed. Eng.* **2015**, *62*, 1457.

[148] B. Schazmann, D. Morris, C. Slater, S. Beirne, C. Fay, R. Reuveny, N. Moyna, D. Diamond, *Anal. Methods* **2010**, *2*, 342.

[149] C. L. Choong, M. B. Shim, B. S. Lee, S. Jeon, D. S. Ko, T. H. Kang, J. Bae, S. H. Lee, K. E. Byun, J. Im, Y. J. Jeong, C. E. Park, J. J. Park, U. I. Chung, *Adv. Mater.* **2014**, *26*, 3451.

[150] R. Li, B. Nie, P. Digiglio, T. Pan, **2014**, DOI 10.1002/adfm.201401527.

[151] D. Y. Park, D. J. Joe, D. H. Kim, H. Park, J. H. Han, C. K. Jeong, H. Park, J. G. Park, B. Joung, K. J. Lee, *Adv. Mater.* **2017**, 1702308.

[152] Y. Joo, J. Byun, N. Seong, J. Ha, H. Kim, S. Kim, T. Kim, H. Im, D. Kim, Y. Hong, *Nanoscale* **2015**, *7*, 6208.

[153] S. C. B. Mannsfeld, B. C.-K. Tee, R. M. Stoltenberg, C. V. H.-H. Chen, S. Barman, B. V. O. Muir, A. N. Sokolov, C. Reese, Z. Bao, *Nat. Mater.* **2010**, *9*, 859.

[154] L. Pan, A. Chortos, G. Yu, Y. Wang, S. Isaacson, R. Allen, Y. Shi, R. Dauskardt, Z. Bao, *Nat. Commun.* **2014**, *5*, 3002.

[155] Y. K. Fuh, B. S. Wang, C.-Y. Tsai, *Sci. Rep.* **2017**, *7*, 6759.

[156] S. Lee, A. Reuveny, J. Reeder, S. Lee, H. Jin, Q. Liu, T. Yokota, T. Sekitani, T. Isoyama,

Y. Abe, Z. Suo, T. Someya, *Nat. Nanotechnol.* **2016**, *11*, 472.

[157] C. Pan, L. Dong, G. Zhu, S. Niu, R. Yu, Q. Yang, Y. Liu, Z. L. Wang, **2013**, DOI 10.1038/NPHOTON.2013.191.

[158] X. Shuai, P. Zhu, W. Zeng, Y. Hu, X. Liang, Y. Zhang, R. Sun, C. Wong, **n.d.**, DOI 10.1021/acsami.7b05753.

[159] B. C. K. Tee, A. Chortos, R. R. Dunn, G. Schwartz, E. Eason, Z. Bao, *Adv. Funct. Mater.* **2014**, *24*, 5427.

[160] S. Wan, H. Bi, Y. Zhou, X. Xie, S. Su, K. Yin, L. Sun, *Carbon N. Y.* **2017**, *114*, 209.

[161] B. You, C. J. Han, Y. Kim, B.-K. Ju, J.-W. Kim, *J. Mater. Chem. A* **2016**, *4*, 10435.

[162] S. C. B. Mannsfeld, B. C. Tee, R. M. Stoltenberg, C. V. H. Chen, S. Barman, B. V. O. Muir, A. N. Sokolov, C. Reese, Z. Bao, *Nat. Mater.* **2010**, *9*, 859.

[163] X. Ding, N. Zhao, G. Yang, R. I. Pettigrew, B. Lo, F. Miao, Y. Li, **2016**, *20*, 1455.

[164] Y. Hodgson, J. Choate, **2012**, 20.

[165] R. Raamat, K. Jagomägi, J. Talts, I. Mäger, **2009**, *31*, 522.